Reconstructing surface mass balance from the englacial stratigraphy of the Greenland Ice Sheet

Alexios Theofilopoulos

Thesis for the degree of Philosophiae Doctor (PhD)
University of Bergen, Norway
2022

UNIVERSITY OF BERGEN

Reconstructing surface mass balance from the englacial stratigraphy of the Greenland Ice Sheet

Alexios Theofilopoulos

Thesis for the degree of Philosophiae Doctor (PhD)
at the University of Bergen

Date of defense: 30.09.2022

Year: 2022

Title: Reconstructing surface mass balance from the englacial stratigraphy of the Greenland Ice Sheet

Name: Alexios Theofilopoulos

Print: Skipnes Kommunikasjon / University of Bergen

Scientific environment

This study is carried out at the Department of Earth Science (Institutt for geovitenskap-GEO), University of Bergen (UIB), Norway. It is part of the project "Modeling Englacial Layers and Tracers in Ice Sheets" (MELT) coordinated by Andreas Born. The work is supported by the Trond Mohn foundation. The PhD candidate has been enrolled in the Bjerknes Centre of Climate Research and the Research school on Changing Climates in the coupled Earth System (CHESS).

Acknowledgements

First and foremost, I would like to thank my supervisor, Andreas Born, for his immense help with my PhD. As a supervisor, he was always available, ready to help and give advice. He followed the progress of the PhD at every single step and his scientific knowledge was very valuable for the whole process. I really thank him because I truly believe that without his help, it would have been impossible for this PhD to be finalized.

I also want to thank the University of Bergen and the Trond Mohn foundation which were providing all the necessary funds. Thanks to them, not only this PhD was possible, but also these four and a half years were a very enjoyable experience, with several travels abroad and within Norway and lots of interactions with international scientists. In addition, I would like to thank the Bjerknes Centre of Climate Research and the Research school on Changing Climates in the coupled Earth System (CHESS) for providing dozens of educational activities.

I also want to thank the department of Earth Science (GEO) and its people for their help, like Øyvind Natvik, Anders Bjørnsen Kulseng and Andrea Grimnes, who were always available to help with IT and administrative problems respectively. Lastly, I want to thank Rebekka Frøystad for her help with the translation of the abstract in Norwegian.

Theofilopoulos Alexios
Bergen, Norway, 10/6/2022

Abstract

The interior of an ice sheet consists of several layers of accumulated snow, whose present thickness depends on the surface mass balance (SMB) of the past and the effect of dynamic thinning after the layer's deposition. This thesis examines the influence that these two factors have on the final stratigraphy of the ice sheet, by using an isochronal numerical ice sheet model. The model, for which SMB is the upper boundary condition, simulates the evolution of the layers through time. The aim of this thesis is to invert the forward model and for a given present stratigraphy to reconstruct the amount of past SMB.

The first part of the thesis uses the isochronal numerical model to examine the influence of SMB on the layer thickness of a two dimensional, idealized ice sheet. The SMB of this idealized simulation is then perturbed at each horizontal location and layer in order to quantify the sensitivity of the layers' thickness to small changes in accumulation, and the results are formalized in a sensitivity matrix. Subsequently, a set of simulations with sustained change in SMB that spans several thousands of years and long distances is performed. In all cases, the impact of SMB is crucial for the stratigraphy of the ice sheet and affects it directly due to changes in SMB itself and indirectly due to alterations of dynamic thinning. The thesis then focuses on recreating the stratigraphy of the simulation with sustained changes in SMB by establishing a linear relation between SMB and layer thickness and extrapolating the sensitivity matrix. The results show that indeed changes in layer thickness due to alterations in SMB can be approximated with a linear relation.

The second part of the thesis focuses on reconstructing SMB from a given layer thickness, the inversion. With the linear system of equations established, its solution is found with three regularization methods, Riley's, Truncated Singular Value Decomposition, and Conjugate Gradient. The SMB reconstruction was performed for the case of an idealized ice sheet with flat bedrock and a 2D meridional cross section of the bedrock of the Greenland Ice Sheet (GrIS) across the ice divide. The results for all cases show an accurate reconstruction of the SMB for all layers at locations close to the ice divide, but the further away from the ice divide, the less layers close to the surface have their SMB accurately reconstructed. This results in a V-shape pattern, where accurate reconstruction of the SMB is only possible within this shape. The thesis concludes with the application of the method on the stratigraphy of GrIS as taken from radiostratigraphy data of NASA's Operation IceBridge.

Abstrakt

Interiøren av isflakene består av mange lag akkumulert snø, hvis tykkelse avhenger av overflatemassebalanse (OMB) fra fortiden og effekten av dynamisk tynning etter lagenes avsetning. Denne oppgaven undersøker påvirkningen disse to faktorene har på den endelige stratigrafien av isflaket ved å bruk av en isokron numerisk isflakmodell. Modellen, som har SMB som en øvre grensebetingelse, simulerer utviklingen av lagene over tid. Målet med oppgaven er å invertere modellen og å rekonstuere mengden av fortidens OMB ved å bruke nåtidens stratigrafi.

Den første delen av oppgaven bruker den isokrone numeriske isflakmodellen for å undersøke påvirkningen av OMB på lagtykkelse av et todimensjonalt, idealisert isflak. OMB fra denne idealiserte simuleringen blir deretter perturbert i hvert horisontale punkt og lag for å kvantifisere følsomhet av lagtykkelse til små forandringer i akkumulering, og resultatene blir formalisert i en følsomhetsmatrise. Etterpå blir et sett av simuleringer med forlenget forandring i OMB som spenner flere tusen år og lange avstander fremført. I alle tilfeller er innvirkningen av OMB sentral til stratigrafien av isflaket og påvirker det direkte på grunn av forandringer i selve OMBen og indirekte på grunn av forandringer i dynamisk tynning. Oppgaven fokuserer deretter på å gjenskape stratigrafien av simuleringen med forlenget forandring i OMB ved å ettablere et lineært forhold mellom OMB og lagtykkelse og ved å ekstrapolere følsomhetsmatrisen. Resultatene viser at virkelige forandringer i lagtykkelse på grunn av forandringer i OMB kan bli tilnærmet med et lineært forhold.

Den andre delen av oppgaven fokuserer i å rekonstruere OMB fra en gitt lagtykkelse, altså inversjonen. Med det etablerte lineære sistemet av ligninger, blir dens løsning funnet med tre regulariseringsmetoder, Riley's, Truncated Singular Value Decomposition, og Conjugate Gradient. Rekonstrueringen av OMB ble utført for tilfellet av et idealisert isflak med flat berggrunn og et 2D meridionalt tverrsnitt av berggrunnen i Grønlands IsFlak (GrIF) over isskillet. Resultatene i alle tilfeller viser en akkurat rekostruering av OMB for alle lag i punkt i nærheten av isskillet, men jo lengre fra isskillet, jo færre lag nær overflaten har en akkurat OMB rekostruering. Dette resulterer i en V-form mønster hvor akkurate rekostrueringer av OMB kun er mulig innenfor denne formen. Oppgaven konkluderer med en applikasjon av metoden for stratigrafien av GrIF som er tatt fra radiostratigrafidata av NASA's Operation IceBridge.

Contents

Chapter 1

Introduction

1.1 Scientific background

Reconstructing past rates of surface mass balance of the Greenland Ice Sheet has been an area of active research for many decades. Already in the 1960s, *Diamond* (1960) created a mapping of precipitation rates from snow profile studies. However, because these snow pits are located at the ice sheet surface, they only provide information for very recent years. In order to reconstruct the paleoclimate, more information is required that goes deeper into the ice sheet. Every ice sheet consists of layers of accumulated snow, each one of which corresponds to different time periods of the past. Layer thickness can be identified in the field via the extraction of ice cores (*Mojtabavi et al.*, 2020) or through ice-penetrating radar (*Legarsky and Gao*, 2006; *MacGregor et al.*, 2015). Regardless of how the data is extracted, it serves as an archive of past accumulation and the cumulative effect of ice flow (*Marshall and Cuffey*, 2000). The thickness of the layers depends on both these factors yet the fact that they act at the same time and often in conflicting ways makes them hard to disentangle. In order to draw a distinct relation between surface mass balance and layer thickness, several approaches have been implemented.

The simplest one is to outright neglect the effect of thinning altogether. This is done usually by calculating average precipitation rates by dividing the current depth of a layer with its age (*Spikes et al.*, 2004), or by simply examining only small changes in accumulation. *Vaughan et al.* (1999), for example examined how variations in accumulation rates affect internal layer features, like troughes and arches. *Morse et al.* (1999) calculated average accumulation by detecting radioactive fallout in order to find depths of stratigraphic horizons. In a similar vein, *Pinglot et al.* (2001) mapped accumulation patterns for one season based on radioactivity of ice cores, again without involving any dynamic thinning. *Pälli et al.* (2002) also estimated the temporal and spatial variability of accumulation rates in Nordenskjoldbreen, Svalbard from ground-penentrating radar. They also neglected layer thinning, but calculated an estimation of the error due to this simplification. The problem with this approach is that it can only be accurate for the very few layers close to the surface, where the effect of dynamic thinning did not have much time to act.

Nye (1963) understood the problem early and introduced a correction factor for what he calls plastic deformation of the ice, in order to quantify the thinning of the layers. *Dansgaard and Johnsen* (1969) built upon Nye and expressed a direct relation between the age of the layer and the initial layer thickness, meaning the precipitation rate, in-

volving a natural logarithm. Their formula became a fundamental tool for layer thinning in several works that followed. The principle of the strain rate has been used for getting precipitation rates from ice cores in Greenland (*Cuffey and Clow*, 1997; *Bales et al.*, 2001) and from radio-echo sounding profiles in Antarctica (*Siegert and Payne*, 2004; *Jacobel and Welch*, 2005; *Huybrechts et al.*, 2009). *Nereson et al.* (2000) estimated spatial distribution of accumulation at Siple-Dome, Antarctica from radio-echo sounding measurements on layers by making small corrections to their parameters and thereby obtaining the best fit. This allowed for the examination of the sensitivity of layer displacement to accumulation changes. Similarly, *Fahnestock et al.* (2001) estimated long term accumulation rates through layer tracing via ice-penetrating radar, by finding an optimized fit using again the model of *Dansgaard and Johnsen* (1969) in Northern Greenland. Fahnestock's misfit parameter was also applied by *Leysinger Vieli et al.* (2004) in East Antarctica. The problem with the simple logarithmic thinning function is that it does not take into consideration horizontal movement of ice. Already, *Paterson and Waddington* (1984) realised the importance of boreholes being taken close to ice divides because, at locations away from it, more complicated models are required.

Two-dimensional models of horizontal ice flow were used to determine the accumulation pattern of East Antarctica (*Siegert et al.*, 2003). They used the concept of balance fluxes and horizontal velocities which are computed from an assumed accumulation rate distribution. The accumulation rates were then adjusted until the modeled isochrones are matched with the internal layers. Similarly, *Baldwin et al.* (2003) calculated mean accumulation patterns by tracing particles backwards on a given field of balance velocities. The velocity field was then updated for the new accumulation rates, and the process is repeated until convergence. The three approaches were summarized by *Waddington et al.* (2007). The shallowest layers follow the Shallow Layer Approximation, and accumulation rates are found by dividing depth with age. Slightly deeper layers follow the Local Layer Approximation. These layers feature dynamic thinning, so a vertical strain rate of 1-D flow is used as a correction. Deeper layers are characterized by horizontal flow and particle trajectories, so complicated models are required for reconstructing surface mass balance. *Waddington et al.* (2007) introduced a proper inversion method for handling those layers. They used a forward model with an ice flow in steady state. Then they created a least squares problem, by finding the model parameters that minimize both the mismatch criterion between model and data as well as the roughness of the expected solution. *Koutnik et al.* (2009) applied Waddington's method for reconstructing accumulation patterns at the polar ice caps of Mars, while *Steen-Larsen et al.* (2010) found multiple solutions for the minimization problem by using a Monte Carlo approach. The importance of horizontal flow for the reconstruction of accumulation rates is evident. *Leysinger Vieli et al.* (2011) made a comparison between reconstructing the surface mass balance for a simple one-dimensional flow model based on Nye, and a full three-dimensional quasi-steady model. They concluded that the inclusion of horizontal advection is indeed important, even in slow flowing areas. Similarly, *Nielsen et al.* (2015), using Waddington's method, solved the inversion problem on a model that included both horizontal and vertical flow, and one that neglected horizontal flow. They concluded that neglecting horizontal flow gives ill-posed solutions for areas near the ice sheet's margins, and large-scale accumulation patterns are more accurately resolved by considering horizontal flow as well.

The method for reconstructing the SMB that we introduce in this project uses an

isochronal numerical model (*Born*, 2017) and bears a lot of similarities with Waddington's inversion method, at least in principle, but not in its assumption of steady state. Surface mass balance and ice flow change through time, their interaction affects the geometry of the internal layers, which in turn affects the slope of the ice sheet's surface, which impacts the subsequent ice flow. In this research we form a system of equations that essentially merge ice dynamics and layer thickness together, at different locations and different time periods. The system of equations is then inverted with regularization techniques in order to reconstruct the surface mass balance.

Chapter 2

Objectives

2.1 Motivation

The objective of this thesis is the development of a method that allows for the reconstruction of the surface mass balance (SMB) by taking into consideration only the Greenland Ice Sheet's (GrIS) stratigraphy. The thesis first focuses on examining how SMB affects the thickness of the internal layers of an ice sheet. It examines the direct effect, through accumulation itself, and the indirect, through changes in dynamic thinning due to the alteration of surface slope. It establishes a way to quantify the sensitivity of layer thickness to changes in SMB and then uses it to linearize the relation between the two, which leads to a formulation of a linear system of equations. The solution of this system serves as the reconstruction of the SMB. The thesis then focuses on identifying an interest area: which layers and locations are the ones whose SMB can be reconstructed. The issues that the thesis addresses are:

- How does SMB impact the thickness of the layers of an ice sheet? (Paper I)
- Can we establish a linear relation between SMB and layer thickness? If yes, how accurate is it? (Paper I)
- How to invert this relation in order to reconstruct the SMB with a given layer thickness? (Paper II)
- How accurate is our reconstruction? The SMB of which layers and horizontal locations can be reconstructed? (Paper II)

2.2 Description of models and data

This thesis uses an isochronal numerical model for simulating explicitely the evolution and movement of the internal layers of an ice sheet (*Born*, 2017). It is applied on a two dimensional grid, representing a cross section of the GrIS (Fig. 2.1). The vertical dimension of the model consists of the isochronal layers themselves, which are equidistant in time, and not in space. New layers are created on top of previous ones, thus growing the computational domain of the model with time. The model's upper boundary condition is SMB, while the model's output is the thickness of the layers in the whole ice sheet domain. All variables of the model advect only horizontally, within each layer, and not

across different layers. Due to the lateral advection, the thickness of the layer changes at each horizontal location, depending on the inflow and outflow of ice mass. Horizontal velocities are calculated via the shallow ice approximation and Glen's flow law and therefore greatly depend on the slope of the ice sheet's surface. The latter one is not constant but instead changes according to the evolution of the layers and the alteration of total ice sheet thickness. This results in an ice sheet which is not on a steady state, but whose ice flow is affected by the ice sheet surface but also affects it through advection and changes in layer thickness.

The increase of the ice sheet is limited by the melt region, on which ice mass is subtracted from the layers. The higher the ice sheet thickness, the more its weight and the more the bedrock below it retreats. Bedrock deformation follows the elastic model of local lithosphere, relaxing asthenosphere (LLRA) (*Le Meur and Huybrechts*, 1996). The boundary condition on the bedrock is no-slip. Additional assumptions include the state of the ice. The model does not describe the firn layers which are usually located near the ice sheet's surface. All layers represented here consist of incompressible ice with density equal to $919.4 kg/m^3$. Different states of water, like liquid, air as well as thermal processes like basal melting or freezing are not considered at all and are outside the scope of this thesis.

The current thesis focuses on developing a method that allows for the reconstruction of the SMB. This method is applied both in idealized cases as well as the real GrIS. As a result real data has been used. Paper II uses data from NASA's Operation IceBridge (OIB) radiostratigraphy data (*MacGregor et al.*, 2021). It is a database of airborne radiostratigraphy records of the englacial stratigraphy of the GrIS (Fig. 2.2). The emphasis is put on a zonal cross section along the ice divide (72.5^o N, 38.3^o W). From all the trajectories of OIB, we use as our data points the locations where the trajectories intersect the parallel 72.5^o N (Fig. 2.3(a)). Some locations which seemed to have unnatural noise were filtered out. We then have a set of internal layers with a specific age (Fig. 2.3(c)) corresponding to a specific elevation (Fig. 2.3(b)). The thickness of the layers is found by subtracting these elevations. Additional data used are the ETOPO1 elevations for the present day bedrock and ice surface (*Amante and Eakins*, 2009). The combination of this data with the LLRA formula allows us to find the elevation of the relaxed bedrock, which is used subsequently as the starting bedrock in our simulations at year 0.

2.3 Formulation of system of equations

The main part of this thesis is the establishment of the method that reconstructs SMB from a given layer thickness. This is done by first formulating a linear system of equations. Assume that we have a target ice sheet (TRG) whose layer thickness is known. This information can be given either from the stratigraphy taken as an output from a simulation, or from real data (radiostratigraphy, ice cores etc.). The question is how to reconstruct the past SMB that created the ice sheet by considering only the layer thickness of TRG. We start by making a very broad estimate of the ice sheet's SMB. The estimate does not need to be accurate, but the closest it is to the correct solution, the easier the next steps become. We use this estimated SMB inside the isochronal layer model and we create a stratigraphy for a new initial ice sheet (INIT). The layer thick-

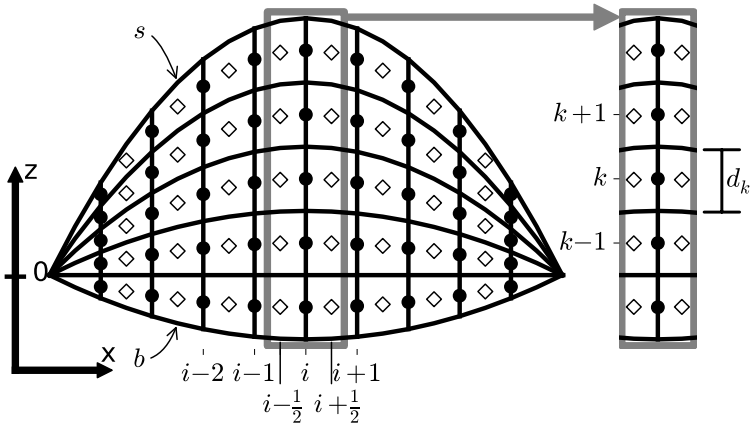

Figure 2.1: Schematic of a 2D cross section of the isochronal layer model. Figure taken with permission from Born (2017).

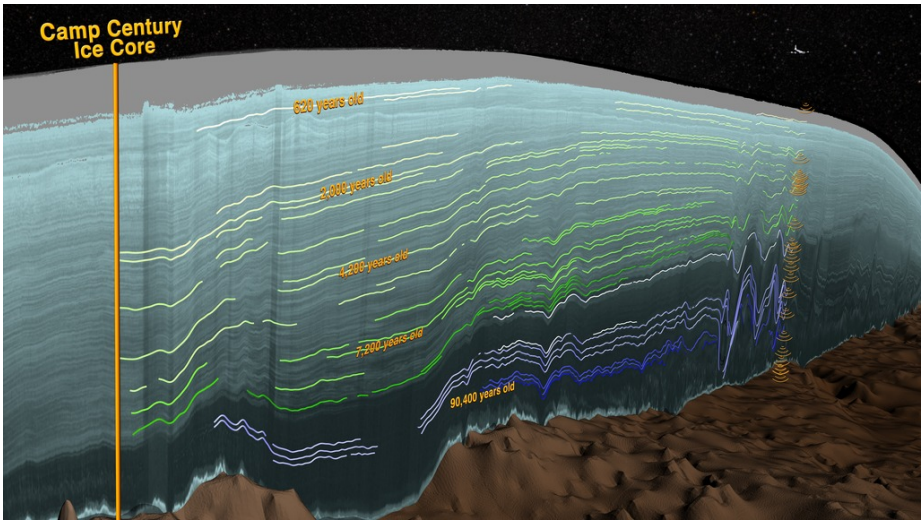

Figure 2.2: Visualization of the internal layers of the GrIS as measured by NASA's Operation Icebridge. Figure taken from NASA's Scientific Visualization Studio (https://svs.gsfc.nasa.gov/4249).

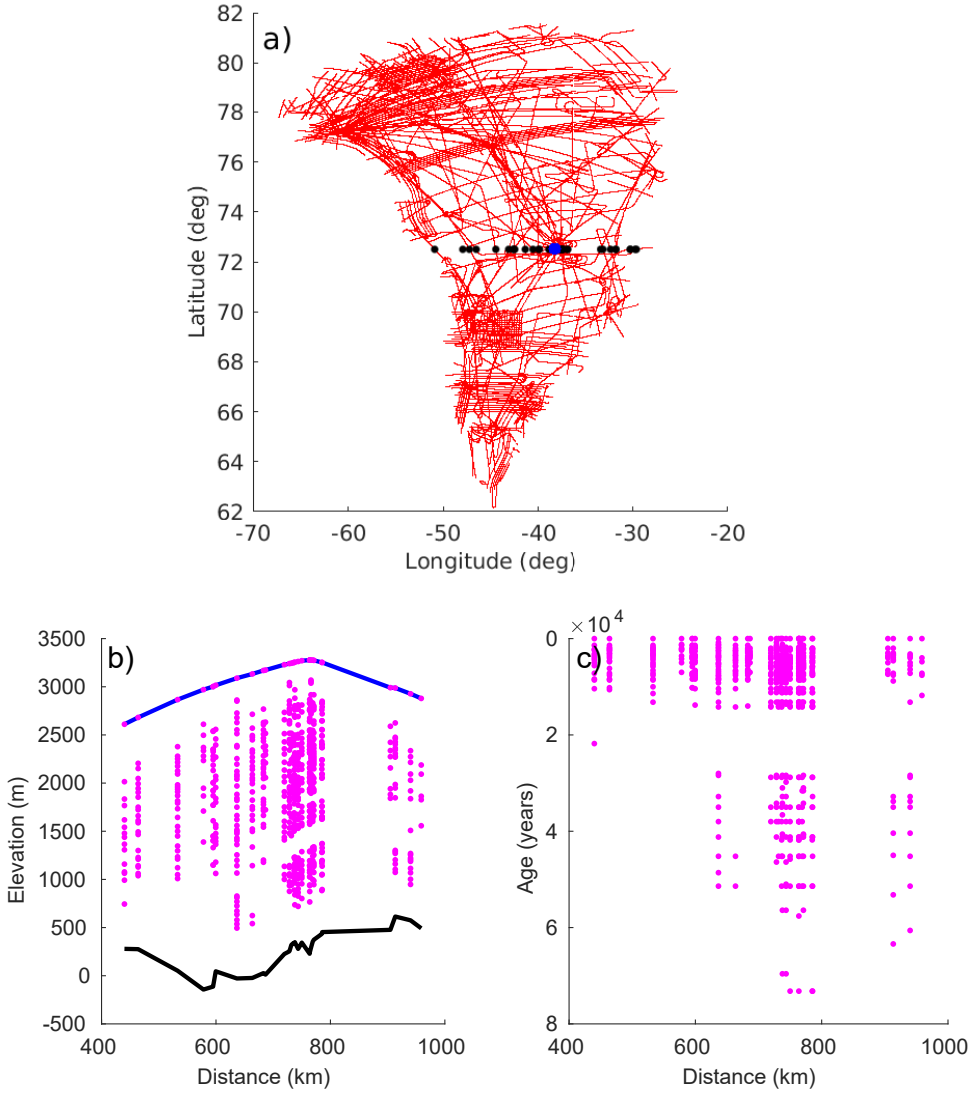

Figure 2.3: Data from NASA's Operation IceBridge. a) Red are the trajectories of all the data, the black dots represent the data columns which we use for our reconstruction. Blue is the location of the ice divide (72.5^o N, 38.3^o W). b) and c) purple are the available internal layers at the longitudinal cross section along the ice divide (72.5^o N), corresponding to the black data points of figure a), the black line is the bedrock and the blue is the ice sheet surface. b) shows the elevation of these layers, while c) the age. Figure taken from Paper II.

ness of TRG can be connected with the layer thickness of INIT by following the Taylor series:

$$d_{TRG,ij} = d_{INIT,ij} + \frac{\partial d_{INIT,ij}}{\partial M_{INIT,i_0 j_0}} \cdot (M_{TRG,i_0 j_0} - M_{INIT,i_0 j_0}) + O(M^2, M^3 ...)$$

where i, j are the horizontal locations and layers that correspond to the specific layer thickness d, while i_0, j_0 are the horizontal locations and layers that correspond to the specific surface mass balance M. Since we are linearizing the relation, we truncate all terms of 2nd order and higher, and the equation turns into the linear approximation:

$$d_{TRG,ij} \approx d_{INIT,ij} + \frac{\partial d_{INIT,ij}}{\partial M_{INIT,i_0 j_0}} \cdot (M_{TRG,i_0 j_0} - M_{INIT,i_0 j_0})$$

The difference in layer thickness $\tilde{d} = d_{TRG,ij} - d_{INIT,ij}$ is known, because the stratigraphy of both ice sheets is known, while the difference in SMB $\Delta M = M_{TRG,i_0 j_0} - M_{INIT,i_0 j_0}$ is uknown because only the SMB of INIT is known. The SMB of TRG is what we are trying to reconstruct. It is important to understand that even though the layer thickness is calculated at a 2D cross section of the ice sheet for specific horizontal locations i and specific layers j, $\tilde{d}$ is actually a vector where all locations and layers have been merged into 1 dimension. Each term of the vector consists of a specific pair of i, j. By that definition, it is:

$$\tilde{d} = \begin{bmatrix} d_{TRG,1} - d_{INIT,1} \\ d_{TRG,2} - d_{INIT,2} \\ .... \\ d_{TRG,m} - d_{INIT,m} \end{bmatrix}$$

with m being the total amount of grid points of the ice sheet domain where layer thickness is measured. For example if the layer thickness data consists of N_i horizontal locations and N_j layers at each location, then $m = N_i \cdot N_j$. Similarly, $\tilde{M}$ is also a vector:

$$\tilde{M} = \begin{bmatrix} M_{TRG,1} - M_{INIT,1} \\ M_{TRG,2} - M_{INIT,2} \\ .... \\ M_{TRG,n} - M_{INIT,n} \end{bmatrix}$$

with n being the total amount of grid points of the ice sheet domain where the unknown SMB is found. It can be $m = n$ but it is not required. The locations with unknown SMB can be different from the locations where the data of layer thickness is taken.

The derivative $\frac{\partial d_{INIT,ij}}{\partial M_{INIT,i_0 j_0}}$ is a measure of how sensitive the layers' thickness of the INIT are for small changes of the SMB, and will be called the sensitivity matrix $\tilde{\sigma}$. This is calculated by making very small perturbations of the input SMB around INIT at all horizontal locations and all layers. For each one of these perturbations, a new simulation is run and the difference in the output of the layer thickness is calculated. Because the derivative needs to be calculated at several locations i_0, j_0 it is a Jacobian matrix and is defined as:

$$\tilde{\sigma} = \begin{bmatrix} \frac{\partial d_{INIT,1}}{\partial M_{INIT,1}} & \frac{\partial d_{INIT,1}}{\partial M_{INIT,2}} & \cdots & \frac{\partial d_{INIT,1}}{\partial M_{INIT,n}} \\ \frac{\partial d_{INIT,2}}{\partial M_{INIT,1}} & \frac{\partial d_{INIT,2}}{\partial M_{INIT,2}} & \cdots & \frac{\partial d_{INIT,2}}{\partial M_{INIT,n}} \\ \cdots\cdots\cdots & & & \\ \frac{\partial d_{INIT,m}}{\partial M_{INIT,1}} & \frac{\partial d_{INIT,m}}{\partial M_{INIT,2}} & \cdots & \frac{\partial d_{INIT,m}}{\partial M_{INIT,n}} \end{bmatrix}$$

The perturbations that are performed around the INIT are very small increases in the amount of SMB. Each perturbation is very local and instaneous, meaning it occurs at each horizontal location and at specific layers, and for every perturbation a new simulation is run. Each column of matrix $\tilde{\sigma}$ represents a new location that has its SMB perturbed, and each row the value of the derivative $\frac{\partial d_{INIT}}{\partial M_{INIT}}$ at that particular grid box of the ice sheet's domain. This value is calculated by subtracting the layer thickness of the INIT from the perturbed INIT and then dividing with the amount of SMB perturbation. Ideally, we would want a separate perturbation at every single layer, but this would require a lot of simulations and could be computationally expensive, so a solution implemented in the thesis is to perturbe the SMB of 3 layers together as a group effectively reducing the temporal resolution. This does not affect the validity of the reconstructed SMB if the equations are scaled appropriately.

To summarize, the relation between layer thickness and SMB is linearized into:

$$\tilde{d} \approx \tilde{\sigma}\tilde{M} \tag{2.1}$$

(2.1) is a linear system of equations and describes a way to linearize the otherwise complicated relation between $\tilde{M}$ and $\tilde{d}$. This linearization is very useful because it allows for an inversion of the problem and solving the unknown $\tilde{M}$, which is mandatory for the reconstruction of the SMB of the TRG. The standard way of solving this kind of systems is:

$$\tilde{M} \approx \tilde{\sigma}^{-1}\tilde{d}$$

However, inverting the sensitivity matrix $\tilde{\sigma}$ is problematic for two reasons. Firstly, it requires that $\tilde{\sigma}$ is a square matrix, meaning $m = n$, and secondly, and most importantly, it is prone to numerical errors. The problem of determining a solution $\tilde{M}$ from a set of values $\tilde{d}$ can be unstable, and then the system is ill-conditioned (*Öztürk and Akdeniz*, 2000; *Ternovski et al.*, 2015). This happens when the condition number of matrix $\tilde{\sigma}$ is too large. The result is that the solution is then corrupted by large amounts of noise.

2.4 Regularization methods

Since inverting $\tilde{\sigma}$ leads to the appearance of great computational noise, in order to find the solution of the system of equations (2.1) regularization methods are required. Three methods are implemented in this thesis: Riley's method, Truncated Singular Value Decomposition and the Conjugate Gradient method.

(1) the *Riley* (1955) method is largely based on the Tikhonov regularization, one of the most common methods for solving ill-conditioned systems (*Hanke and Groetsch*, 1998; *Calvetti et al.*, 2003; *Reichel et al.*, 2012; *Donatelli and Reichel*, 2014; *Xingsheng et al.*, 2015). If a strict mathematical solution for the system (2.1) does not exist, or is

not stable, a best fit solution $\tilde{M}$ can be found, by minimizing the least squares problem (*Bjorck*, 1991):

$$\min_{\tilde{M}}\{||\tilde{\sigma}\tilde{M} - \tilde{d}||^2\}$$

On their own, least squares problems do not address unstable solutions, but the Tikhonov regularization adds an additional term transforming the minimization problem into:

$$\min_{\tilde{M}}\{||\tilde{\sigma}\tilde{M} - \tilde{d}||^2 + \lambda||Z\tilde{M}||^2\} \tag{2.2}$$

The addition of the filtering term $\lambda||Z\tilde{M}||^2$ forces a solution $\tilde{M}$ that not only minimizes $||\tilde{\sigma}\tilde{M} - \tilde{d}||^2$, but the filtering term as well. The way the filter is implemented differs according to the choice of the Z matrix, but if it is taken equal to the identity matrix I then the Tikhonov regularization is said to be in standard form, and the filtering factor becomes $||I\tilde{M}||^2 = ||\tilde{M}||^2$ which essentially is satisfied for low absolute values of $\tilde{M}$. By forcing $\tilde{M}$ to be as low as possible, the large amounts of noise are filtered out, and $||\tilde{\sigma}\tilde{M} - \tilde{d}||^2$ is minimized for a solution that does not include noise. The factor λ plays the role of regulating the dominance of the filtering term $||\tilde{M}||^2$ over the minimization problem $||\tilde{\sigma}\tilde{M} - \tilde{d}||^2$. If λ is close to 0, then no filter exists and the problem is the same as if no Tikhonov regularization applies. If λ approaches infinity then there is no minimization problem to be solved and as a result $\tilde{M} = 0$.

The solution of $\tilde{M}$ that minimizes (2.2), is found equal to (*Twomey*, 1963; *Heath*, 1974; *Hochstenbach and Reichel*, 2010; *Reichel et al.*, 2012; *Donatelli and Reichel*, 2014):

$$\tilde{M} = (\tilde{\sigma}^T\tilde{\sigma} + \lambda I)^{-1}\tilde{\sigma}^T\tilde{d}$$

The choice of the weighting factor λ impacts the results, but there is no definite answer for an ideal value of it. One of the most widely used methods for the most suitable λ is the L-curve method (*Hansen and O'leary*, 1993; *Calvetti et al.*, 2000; *Kilmer and O'Leary.*, 2001). Here, we will use a variation of the Tikhonov regularization, an iterative scheme proposed by *Riley* (1955), whose sequence converges to the least squares solution for any $\lambda > 0$ (*Golub*, 1965; *Heath*, 1974; *Spigler*, 2020):

$$\tilde{M}^{i+1} = (\tilde{\sigma}^T\tilde{\sigma} + \lambda I)^{-1}(\tilde{\sigma}^T\tilde{d} + \lambda\tilde{M}^i)$$

(2) the Singular Value Decomposition (SVD) is a way to factorize any $m \times n$ matrix. The difference between SVD and other factorization methods, like the LU decomposition, is that it is not required for the matrix to be symmetric or square. With the SVD, the sensitivity matrix σ is factorized into:

$$\tilde{\sigma} = U\begin{pmatrix} Q \\ 0 \end{pmatrix}V^T$$

where $\begin{pmatrix} Q \\ 0 \end{pmatrix}$ is a $m \times n$ matrix with the only non zero values being the diagonal elements $Q = diag(q_1, q_2, q_3, ...)$, where q_1, q_2, q_3 are the square roots of the eigenvalues of the matrix $\tilde{\sigma}^T\tilde{\sigma}$, also known as singular values, with $q_1 \geq q_2 \geq q_3 \geq ... \geq q_n$. The matrix V consists of the orthonormalized eigenvectors of $\tilde{\sigma}^T\tilde{\sigma}$ while the matrix U consists of the

orthonormalized eigenvectors of the n largest eigenvalues of $\tilde{\sigma}\tilde{\sigma}^T$ (*Varah*, 1973; *Stewart*, 1993). By using the factorization on system (2.1), we have:

$$\tilde{d} \approx U \begin{pmatrix} Q \\ 0 \end{pmatrix} V^T \tilde{M}$$

whose solution is (*Golub and Reinsch*, 1970; *Heath*, 1974):

$$\tilde{M} = V \left(Q^+, 0\right) U^T \tilde{d}$$

where $Q^+ = diag(q_1^{-1}, q_2^{-1}, q_3^{-1}, ...)$. The expression can also be written out explicitely as:

$$\tilde{M} = \sum_{i=1}^{n} \frac{u_i^T \tilde{d}}{q_i} v_i \tag{2.3}$$

The terms in the summation (2.3) appear in a decreasing singular value order, with $q_1 \geq q_2 \geq q_3 \geq ... \geq q_n$. The later terms are smaller and since they are on the denominator, the solution will give very large values. The inclusion of these smaller terms is responsible for the appearance of the noise on the non-regulated solution. In order to regulate it, we need to truncate the terms of the summation (2.3) to a $k \leq n$. This is called the Truncated Singular Value Decomposition (TSVD) (*Heath*, 1974; *Hansen*, 1990). This way, the solution only keeps the important terms of the summation, the ones that minimize the problem, and not the terms that create the noise.

(3) the Congugate Gradient algorithm (CG) is an iterative way of solving the linear system of equations (2.1) (*Calvetti et al.*, 2003). $\tilde{M}$ can be analyzed into a basis of conjugate vectors p_i with respect to the sensitivity matrix $\tilde{\sigma}$. This means that $p_i^T \tilde{\sigma} p_j = 0$ for all $i \neq j$. It can thus be written:

$$\tilde{M} = \sum_{i=1}^{n} a_i p_i$$

The next step is to find the conjugate vectors that form the basis p_i and their factors a_i. The least squares solution of the system $\tilde{d} \approx \tilde{\sigma} \cdot \tilde{M}$ is equivalent to solving $\tilde{\sigma}^T \tilde{d} = \tilde{\sigma}^T \tilde{\sigma} \cdot \tilde{M}$. The residual $p_0 = \tilde{\sigma}^T \tilde{d} - \tilde{\sigma}^T \tilde{\sigma} \cdot \tilde{M}_0$ is taken as the first conjugate vector, where M_0 is a first approximation of the solution. The a_i and the rest of the conjugate vectors p_i can be found iteratively by following an algorithm (*Bjorck*, 1991; *Brufati et al.*, 2016):

Define $M_0 = 0$ *as the initial approximation of the SMB:*
$\tilde{r_0} \leftarrow \tilde{d} - \tilde{\sigma} \cdot \tilde{M_0}$
$\tilde{z_0} \leftarrow \tilde{\sigma}^T \cdot \tilde{r_0}$
$\tilde{p_0} \leftarrow \tilde{z_0}$
For a set of k iterations, it will be:
$\tilde{w_k} \leftarrow \tilde{\sigma} \cdot \tilde{p_k}$
$a_k \leftarrow \left(\tilde{z_k}^T \tilde{z_k}\right) / \left(\tilde{w_k}^T \tilde{w_k}\right)$
$\tilde{M}_{k+1} \leftarrow \tilde{M_k} + a_k \cdot \tilde{p_k}$
$\tilde{r}_{k+1} \leftarrow \tilde{r_k} - a_k \cdot \tilde{w_k}$
$\tilde{z}_{k+1} \leftarrow \tilde{\sigma}^T \cdot \tilde{r}_{k+1}$
$\beta_k \leftarrow \left(\tilde{z}_{k+1}^T \tilde{z}_{k+1}\right) / \left(\tilde{z_k}^T \tilde{z_k}\right)$

$\tilde{p}_{k+1} \leftarrow \tilde{z}_{k+1} + \beta_k \cdot \tilde{p}_k$

From these regularization methods, the SMB of TRG is found. In order to further optimize the solution, the reconstructed SMB can be used as a new SMB in order to define a new INIT ice sheet. Then a new $\tilde{\sigma}$ is calculated around the new INIT and by applying the regularization methods on the new system of equation, we can get a new reconstructed SMB. This new reconstructed SMB is closer to the correct solution than the first approximation, because this time the ice sheet was initialized by using an SMB that was the result of the first approximation. This means that the distance between TRG and INIT in the Taylor expansion is smaller and thus the linearization (2.1) more accurate. By repeating the same process several times, we keep making the linearization more accurate and the reconstructed SMB closer to the correct solution. These optimization loops exist as a way to address the non-linearity of the model. While the system of equations is a linearized approximation, by updating this system with more accurate variables, this approximation becomes more and more representative of the non-linear behavior.

Chapter 3

Summary of the papers

Paper I: Sensitivity of isochrones to surface mass balance and dynamics

Theofilopoulos & Born, Journal of Glaciology, accepted

The interior of an ice sheet consists of layers of accumulated snow, also known as isochrones. The layers' thickness during the time of deposition is equal to the amount of surface mass balance (SMB), however, with the passing of time, this thickness experiences dynamical thinning via the flow of ice. Paper I examines the sensitivity of the layers' thickness to changes in SMB. These changes affect the layer thickness in two ways: directly through changes in precipitation, and indirectly through the impact in the dynamical behavior of the ice sheet, caused by changes in the slope of the ice sheet surface. The project uses an isochronal layer ice sheet model, which explicitely simulates the englacial stratigraphy of a 2D cross section of an ice sheet. Two sets of simulations are performed around a control simulation. The first set consists of a series of infinitisemal perturbations of SMB around all layers and all horizontal locations of control, in order to quantify how sensitive the layer thickness of the ice sheet is to very small, local and instaneous changes in SMB. The result of the simulations is stored in a sensitivity matrix. The second set consists of sustained changes in SMB that impact the layer thickness for large areas and for long periods of time. The project then focuses on recreating the layer thickness of the second set of simulations, by using only the sensitivity simulations of the first set. This is done by establishing a linear relation between SMB and layer thickness via the sensitivity matrix. The relation is then extrapolated for a given deviation of SMB from the control simulation. The paper concludes that linearity is a good representation of the relation between SMB and layer thickness, and it can potentially allow for a future inversion of the relation in order to reconstruct past SMB.

Paper II: Reconstructing the surface mass balance from Greenland's ice sheet stratigraphy

Theofilopoulos & Born, Journal of Glaciology, submitted

Paper II focuses on solving the linear system of equations Paper I established, in order to find the unknown SMB for a given layer thickness. This allows for the reconstruction of paleoclimate by using as the only information the stratigraphy of the ice sheet. In order to test the quality of the reconstruction method, the isochronal numerical model

is used to first simulate a target ice sheet and the SMB of the target is reconstructed. A second ice sheet is used as a reference, an initial, and the layer thickness of both the initial and the target as well as the SMB of the initial get imported inside the system of equations in order to get a solution for the only unknown, which is the SMB of the target. Because the system is ill-determined, three different regularization methods were used in order to solve it, Riley's method, Truncated Singular Value Decomposition and the Conjugate Gradient method. The solution can also be optimized by redefining the initial simulation, recalculating a new sensitivity matrix based on the first inversion result and repeating the process until convergence. The inversion method manages to reconstruct the SMB quite accurately for locations close to the ice divide. The further away from the ice divide, the less years before present are accurately reconstructed. The result is a V-shape pattern on the isohcronal grid, where all layers inside this shape have their SMB well reconstructed. This occurs because locations outside the V-shape experience strong dynamic thinning and their SMB does not affect significantly the final stratigraphy of the ice sheet, making it impossible to recover information from them. In addition, this work examines how the resolution and scarcity of layer thickness data can affect the reconstructed SMB. A fine grid of data gives a smooth solution, while a coarser grid with gaps is more susceptible to noise. Subsequently, Paper II applies the reconstruction method on a 2D cross section across of the real Greenland Ice Sheet (GrIS) at 72.5^o N. The available layer thickness is taken from radiostratigraphy data of NASA's Operation IceBridge. The solved SMB is polluted by noise, a result of the scarce IceBridge data used, but comparing the reconstructed SMB at 72.5^o N, 38.3^o W with the precipitation data from the GISP2 ice core at the same location gives similar results for the last thirty thousand years, with the Holocene and the Last Glacial Maximum reconstructed quite accurately, despite the limitations of the 2D model.

Chapter 4

Scientific results

Paper I

Sensitivity of isochrones to surface mass balance and dynamics

Theofilopoulos Alexios, Born Andreas
Journal of Glaciology, accepted

Sensitivity of isochrones to surface mass balance and dynamics

Alexios THEOFILOPOULOS,[1,2] Andreas BORN,[1,2]

[1]*Department of Earth Science, University of Bergen, Norway*

[2]*Bjerknes Centre for Climate Research, Bergen, Norway*

ABSTRACT. The interior of an ice sheet consists of layers of accumulated snow, which contain important information on accumulation and ice dynamics that are imprinted on layer shapes over time. This work describes how changes in accumulation influence the stratigraphy of an ice sheet. The thickness of each layer at present day depends both on accumulation as well as the effect of dynamic thinning after its deposition. An isochronal numerical model is used to simulate the evolution of a two dimensional, idealized ice sheet while explicitly representing the layers. A series of simulations was carried out to quantify the changes that anomalous accumulation at different locations and times has on the stratigraphy. These simulations form the basis of a linear response function. A second set of simulations with more sustained changes in accumulation is then used to describe large scale and long term impacts on the layering of the ice sheet as well as to test the quality of the linear approximation. The aim is to examine whether long term effects can be extrapolated from small differential changes. The result confirms a certain degree of linearity between changes in accumulation and layer thickness that may be exploited for future inverse modeling applications.

1. INTRODUCTION

The interior of major ice sheets is characterized by a stratigraphic record of distinct layers of equal age, also called isochrones, which, in the field can be identified in several ways, including the extraction of ice cores (e.g. Mojtabavi and others, 2020) and the use of ice penetrating radar (e.g. Legarsky and Gao, 2006; MacGregor and others, 2015; Winter and others, 2019). The present day thickness of these layers is a result of past accumulation and the cumulative effect of ice flow, two factors that in reality are hard to separate. In the past, attempts have been made to describe a direct relation connecting surface mass balance (SMB) to layer thickness, by finding ways to simplify the effect of ice flow. For shallow layers and far from regions of active ice flow, the dynamic effect on layer thinning can be neglected and an average precipitation rate can be found by dividing the current depth of a layer with its age (e.g. Pinglot and others, 2001; Spikes and others, 2004; Medley and others, 2013). A more sophisticated approach introduces a correction factor for the thinning of the layers (Nye, 1963), thus connecting SMB with layer thickness via a natural logarithm (Dansgaard and Johnsen, 1969). This involves a 1-D flow model, neglects horizontal advection and introduces a constant strain rate in order to calculate a mean accumulation rate (Cuffey and Clow, 1997; Leysinger Vieli and others, 2004; Siegert and Payne, 2004; Huybrechts and others, 2009).

These approaches require considerable simplifications of the ice dynamics and are only accurate for shallow layers. At the same time however, attempts to simulate deeper isochronal surfaces have also been made with full thermomechanical ice sheet models. The inclusion of an Eulerian tracer for the age since deposition is relatively easy to do, but requires the introduction of artificial diffusion that negatively affects the results (Greve, 1997; Born and Robinson, 2021). A Lagrangian approach is also possible (Rybak and Huybrechts, 2003; Sutter and others, 2021) and produces more accurate results, but requires interpolation procedures between grid-points, which over time accumulate errors and add complexity. To circumvent this complication, Tarasov and Peltier (2003) introduced a semi-Lagrangian transport scheme that back-tracks tracer trajectories onto the Eulerian grid at every time step. This approach may be further improved by using depositional provenance markers instead of individual tracers, because the provenance marker field is relatively smooth in space and therefore less prone to interpolation errors (Clarke and Marshall, 2002; Clarke and others, 2005; Goelles and others, 2014).

Given that complex 3-D models that simulate ice tracer flow exist, the question now is whether these can be used in order to replace the 1-D strain rate formula of Dansgaard and Johnsen (1969) and generalise the direct link between layer thickness and SMB for deeper layers as well, while also considering horizontal

flow. Baldwin and others (2003) calculated mean accumulation patterns by tracing backwards ice particles within a given field of balance velocities. Waddington and others (2007) formulated a least squares inversion problem in order to link directly layer thickness with the smoothest SMB that minimized the misfit between data and model. Comparisons between 3-D and 1-D models show that horizontal ice flow is indeed important and prefferable to be taken into consideration (Leysinger Vieli and others, 2011; Nielsen and others, 2015). However, because these studies also require a given velocity field, the ice sheet evolution is considered to be on a steady state.

This study connects directly SMB and layer thickness with the help of an isochronal layer model (Born, 2017). The model treats the discretization of the vertical axis not as a grid that is fixed in space, but rather as individual layers corresponding to different times. The explicit simulation of each layer allows for a continuous calculation of ice sheet thickness and surface slope, meaning that ice flow is constantly updated and the ice sheet is not on a steady state. This means that a perturbation of SMB will trigger a response from ice dynamics and will leave a footprint in the thickness of the isochronal layers. The project focuses on using the isoschronal model in order to establish a linear relation between SMB and layer thickness. By doing so, ice flow is parameterized inside this linearization formula and thus changes in layer thickness can then be approximated directly from changes in SMB. This is very useful for a future inversion of the problem, which will allow for the reconstruction of the SMB based on available data of the internal layers of ice sheets. This is not an easy problem, because it requires the use of regularization methods in order to find a least squares solution, however, an additional method for simplifying the relation between SMB and layer thickness is worth analysing, since the reconstructed SMB will serve as supplementary information on variability in the hydrological cycle, complementing water isotope tracers (e.g. Noon and others, 2003; Lasher and others, 2017).

Section 2 gives a brief description of the model used for this analysis and the simulations performed in order to establish the linearization between SMB and layer thickness. Section 3 puts this relation into test in order to check its accuracy. We find that, within certain limits, the linear reconstruction is representative of the behavior that SMB perturbation has on layer thickness. Section 4 attempts to use this linear function in order to reconstruct SMB for a given layer thickness. Lastly, section 5 describes the conclusions of this analysis and gives some remarks of how to expand on the linearization in future work.

2. METHODS

2.1. Model description

The model used for the present analysis is an isochronal layer model that simulates the evolution and movement of layers of accumulated snow in the interior of an ice sheet (Born, 2017). This means that all variables, including layer thickness, are advected horizontally, but only within each layer and not across isochronal horizons. The vertical dimension consists of the isochronal layers. The model grid consists of layers that are not equidistant in space, but instead they are in time. Every 200 years a new layer is added on top of the ice sheet, thus increasing the computational domain of the model during run time. Due to lateral advection, the layers' thickness changes with time at each location, and is directly connected to the mass that is advected horizontally within the layer. None of the variables are advected vertically through the isochronal grid. Vertical movement is solely due to thinning of older layers below. Horizontal velocities are calculated by using the shallow ice approximation and Glen's flow law. All variables, including layer thickness, are advected using a first order implicit scheme. In the ablation zone, where SMB is negative, the layers melt and their thickness is reduced accordingly. Horizontal velocities depend primarily on the slope of the ice sheet surface, which is calculated anew at each time step of the model. This means that ice flow is also changing during the simulation and the ice sheet is not in a steady state. The time dependance of the model allows us to emphasize and examine the long term response of layer thickness to changes in SMB. The model does not represent the firn layer on top of the ice sheet and processes at the ice sheet bed, e.g. basal freeze-on are not included although they may have a significant effect on the stratigraphy at depth (Leysinger-Vieli and others, 2018). Note that this work prioritizes uncertainty in boundary conditions, specifically accumulation, and deliberately omits the also important uncertainty in other model parameters. While both are equally important and influence each other, we choose to separate our work in studies of parameter uncertainty (Born, 2017; Born and Robinson, 2021) and the present study.

For the current project, the model domain is chosen to represent a two-dimensional cross section of the GrIS at the ice divide spanning 133 points laterally with a spacing of 10 km (Fig. 1d). The reference point 0 km will be set at the location of the ice divide. The model has recently been updated to a 3D version that represents the isochrones of the entire Greenland Ice Sheet (Born and Robinson, 2021). This new version improves the numerical efficiency by decoupling the layer tracing scheme from the simulation of ice physics, where the latter are carried out on the much coarser grid of the host model. However, since the two-dimensional advection equation still has to be solved for every isochrone, the 3D simulation for

the entire Greenland domain is more expensive than the zonal section presented in Born (2017). This simplification does not impact the validity of our results.

2.2. Description of simulations

Two sets of simulations are conducted which differ in the prescribed SMB and the response of the bedrock to changing ice load (Table 1). The simulations are idealized with a flat bedrock and a constant flow factor of $1.397 \cdot 10^{-24} Pa^{-3} s^{-1}$, which corresponds to a temperature of $-5^{o}C$ (Cuffey and Paterson, 2010; Born, 2017). We chose a relatively high value to represent the region where most deformation takes place, near the ice sheet bed. Since temperatures are closer to the melting point near the bedrock (Johnsen and others, 1995), we chose this temperature in order to increase the ice flow of the simulated ice sheet within realistic boundaries. Temperature and therefore ice viscosity are constant everywhere in an effort to limit the number of free parameters. Note that this idealized setup is chosen to approximate an ice sheet with the physical and geographical characteristics of the Greenland ice sheet, but does not attempt a faithful reproduction of all details. At the upper boundary, we apply an idealized SMB, representing a net effect of accumulation minus melting. The bedrock subsides under the weight of the ice sheet as described by the local lithosphere, relaxing asthenosphere (LLRA) model with a time scale of 10,000 years (Le Meur and Huybrechts, 1996). At the begining of the simulations, no ice is present, so the bedrock is relaxed. All simulations span 200,000 years so that the vertical isochronal dimension contains 1,000 layers at the end of the simulation (a new layer every 200 years). The first 150 kyr are common for all simulations and the SMB follows a simple parabolic distribution to reach a steady state before the onset of the SMB anomaly, at which point the ice sheet is not on a steady state anymore, and this is the period that mostly interests us. The SMB is positive between -180 and 180 km, where precipitation dominates, (Fig. 1a), while outside this region the parabolic has negative SMB, and melting dominates (Fig. 1b). After 150 kyr, the total ice volume is stable (Fig. 1c) indicating that a steady state condition has been reached. A control simulation (**CTRL**) is carried out, in which the reference isochronal state of the ice sheet is established. CTRL is run with constant parabolic SMB forcing for 200 kyr.

The first set of simulations aims to establish a sensitivity matrix, comprising of parameters that quantify the sensitivity of the thickness of the isochronal layers to very small SMB anomalies. These sensitivity simulations consist of very small perturbations of the SMB around CTRL, both local and short-lived, meaning they only affect one layer at one particular location, a single grid box. Only locations of positive SMB are perturbed, of which there are 40 equidistant ones between -180 km and 180 km. Perturbations are

applied for all layers between 150 kyr and 200 kyr, layers 751 - 999 for a total of 9,960 simulations (layer 1,000 is not considered because it is created as soon as the simulation ends and has no impact on layer thinning). At each location, the perturbation is defined as an increase of SMB by 1/1000th of CTRL at the same location. Since perturbations are applied to all locations and layers, all results are accumulated in a sensitivity matrix. The 9,960 sensitivity simulations are used for the calculation of the sensitivity parameter σ, which is defined as the increase in layer thickness caused by the infinitesmal increase of SMB by 1/1000th and is given by:

$$\sigma_{i_0 \cdot N + j_0, i \cdot N + j} = \frac{\partial d_{i,j}}{\partial M_{i_0,j_0}} = \frac{d_{i,j} - d_{CTRL,i,j}}{\frac{1}{1{,}000} M_{i_0,j_0}} \tag{1}$$

where d is the thickness of layer j at horizontal location i of the sensitivity simulations, d_{CTRL} is the thickness of layer j at location i of the CTRL simulation, $\frac{1}{1000}M$ is the amount of net SMB perturbation per layer (200 years) at location i_0 for the layer j_0 according to the parabolic distribution, and $N = 249$ are the total amount of layers. σ is essentially a metric of how a perturbation conducted at each of the 40 locations and each of the 249 layers affects the thickness of all layers at all locations. For each one of these 9,960 sensitivity simulations, σ contains the normalized values of the thickness difference at all locations and all layers, which are also 9,960, making σ a matrix with dimensions $9,960 \times 9,960$. If $\sigma_{i_0 \cdot N + j_0, i \cdot N + j}$ is positive then a positive perturbation at i_0, j_0 creates a thicker layer at i, j for the perturbed simulation over the CTRL, while if the value of σ is negative, then a positive perturbation at i_0, j_0 creates a thinner layer at i, j.

The second set of simulations consists of more sustained changes in SMB from CTRL. The emphasis is put again on analyzing how these affect the thickness of the layers. The changes in SMB last longer, span larger areas and entail either an increased or a decreased anomaly of the SMB. In a third case the SMB oscillates between these increased and decreased anomalies. The anomalies are limited to one section of the ice sheet, in order to examine if the thickness of the layers is affected only downstream or whether there is an impact on the isochrones across the ice divide as well.

The simulation with increased SMB (**SMB+**) is based on CTRL for the first 150 kyr, followed by the increased SMB distribution between 150-200 kyr. The increase is centered around 80 km and follows a cosine function, with an amplitude of 0.01 m/yr (Fig 1a). In the simulation with reduced SMB (**SMB-**) the identical spatial and temporal anomaly pattern as in SMB+ is applied, but this time with a negative SMB anomaly of the same size. A third simulation uses an oscillating SMB (**OSC**) after the spin-up. It

Table 1. The SMB distribution of all simulations on each time period.

Simulation	0 - 150 kyrs	150 - 200 kyrs
CTRL	Parabolic	Parabolic
Sensitivity Simulations	Parabolic	1/1000th SMB increase in a single grid box
SMB+	Parabolic	Increased
SMB-	Parabolic	Reduced
OSC	Parabolic	Oscillatory
CTRL Non-deformable bedrock	Parabolic	Parabolic
SMB+ Non-deformable bedrock	Parabolic	Increased
SLID	Parabolic	Parabolic

oscillates between the increased and reduced SMB distributions with a period of 5 kyr, following a sine function so that between 150-200 kyr there are a total of 10 full oscillations. In contrast to SMB+ and SMB- where the total amount of precipitation differs from CTRL, OSC has the same total SMB as CTRL.

Two additional simulations were conducted with SMB distribution identical to the CTRL and SMB+ whose bedrock, instead of being deformable, remains flat for the whole period of the simulations. The simulations were performed in order to differentiate the effects that the bedrock itself has on the internal layers from the effects of dynamics and SMB. These two simulations are only performed in order to explain a very specific signal of the age difference located in the bottom layers of the ice sheet. Since they do not contribute to anything more in the results described below, there is no reason to expand these simulations for the cases of SMB– and OSC.

Lastly, we also examined briefly the impact of sliding (**SLID**). We ran one more simulation, identical to the CTRL when it comes to the distribution of SMB, but between 170,991-171,000 years, we activated a constant sliding at 130 km of 10^{-6} m/s.

3. RESULTS

3.1. Sensitivity simulations

The σ matrix containing the values of the sensitivity parameter can be visualized in two ways: First, by showing the effect that the perturbation of SMB of a particular layer at a particular location has over the whole ice sheet, and, secondly, by showing how the perturbation at all possible locations and layers of the ice sheet affects one particular location and layer.

It is important to understand that when a perturbation of SMB occurs at a very specific location and layer, it still affects the layer thickness of all layers at all locations. This is a result of the ice sheet reacting to the change of dynamic thinning caused by the small perturbation. By quantifying this response, we can parameterize the effect of dynamic thinning. This quantification is stored in the sensitivity matrix. As an example, the value of the sensitivity matrix when the perturbation occurs at location 80 km and layer 850, corresponding to a SMB perturbation at 170 kyr, is visualized at the end of the simulation (200 kyr, Fig. 2a). All the anomalies shown here are caused by a combination of the direct reaction due to the increase in SMB and an indirect due to changes in dynamic thinning. A complex pattern of layer thickening and thinning results from this simple small SMB perturbation, with most changes occuring below the perturbed layer. These anomalies can also be seen in the time domain, i.e., the model grid, which we will use for further discussions (Fig. 2b). Unlike the spatial domain, where results get distorted by different elevation changes in different simulations, the time domain allows for a direct comparison of the isochronal layers between the different simulations.

The direct effect of the increase in SMB is very local and can only be found directly downstream of the perturbed layer (layer 850) (Fig. 2c). The signal of the increased thickness extends to the whole downstream section of the perturbed layer (locations $>$ 80 km), a result of the increased ice mass being transported towards the margins by the flow, thus increasing the thickness of the layer at all downstream locations.

The layers below the perturbed layer (areas 3 and 4 of Fig. 2b) show a dual signal of increased and decreased thickness. The border between the two (located in area 3) is not constant and for younger layers it is moved more to the right than for older layers. The dual signal of this region is a result of the alteration in surface gradient created by the increase in SMB at layer 850. Because of the increase in SMB of the perturbed layer, the total thickness of the ice sheet at location 80 km as well as the gradient downstream, increases. This causes an increase in the downstream velocities that forces more mass transport. Consequently, the layers below the perturbation become thinner due to more ice loss. The negative sensitivity extends on the whole downstream section of the ice sheet up to the right margin. Upstream of location 80 km (area 4) layer thicknesses increase. Because of the local increase in elevation at 80 km, the gradient from the ice divide to 80 km decreases, reducing the horizontal velocities there. The layers there lose less ice mass and remain thicker. The reason why the border separating the two signals is not at the same location for all layers but instead is more to the right for the younger layers is related

to the flow of ice. Since horizontal velocity is greater for younger layers, the signal is advected faster and moves faster towards the right margin when compared to the layers closer to the bed.

Layers younger than the perturbation (areas 1 and 2) are also affected and generally show a reduction in ice thickness. This is a result of the increase in surface slope caused by the anomalous accumulation in older layers. The resulting anomalies in dynamic thinning outlast the direct effect of higher accumulation rates and therefore also impact layers that are deposited after the perturbation period. Since the downstream part below the perturbed layer has thinner layers while the upstream part has thicker layers, the slope of the surface is expected to increase. This increases the dynamic thinning and produces thinner younger layers. The ice mass is then advected towards the right margin, slightly increasing the thickness of the layers at this location.

It is interesting to note that the perturbation at 80 km, layer 850 also affects the locations < 0 km with a similar pattern as for the region between the ice divide at 0 km and up to 80 km. This can be explained if one considers the relation between the two regions. Between 0-80 km, older layers remain thicker (area 4). Thicker layers on one side of the ice divide mean that more mass is transported to the opposite side to locations < 0 km. As a result, the layers of these locations remain thicker as well. For the younger layers of locations 0-80 km (area 1), which are thinner, the layers accumulate less mass near the ice divide, and thus less mass also flows at locations < 0 km. It becomes clear that a perturbation on one side of the ice sheet, despite how small it might be and despite the fact that it does not create a horizontal movement of the location of the ice divide, still affects the layering of the ice sheet as a whole. Because layer thickness, horizontal velocities and surface slope are all factors that interact at all times, a small change of SMB affects the physical mechanism of ice flow not only around the point of the perturbation, but instead leaves its impact in the whole ice sheet, even including the section at the opposite side.

The sensitivity matrix can also provide information about another question: How do the perturbations at all possible horizontal spatial locations and all layers of the ice sheet affect one particular location and layer? As an example, the effect that perturbations at all locations and layers have on location 80 km and layer 850 are shown in figure 3. Since only layers younger than 750 were perturbed, the sensitivity to SMB changes before that (1-750) is unknown and therefore not shown here. The vertical axis in figure 3 is labeled as the perturbed layer, which directly corresponds to the accumulation time when the perturbation occured. The best way to read this slice of the sensitivity matrix is by associating each entry with the SMB of a certain point in space and time. So for example, at location 100 km and layer 950, we see how a

perturbation at 100 km and 190 kyr into the simulation affects the thickness at location 80 km, layer 850, at the end of the simulation. Layer 850 increases in thickness by perturbations that occur upstream from location 80 km in the same layer, because these changes are advected towards location 80 km. Perturbations that occur on older layers (751-849) have a primarily negative effect on the layer thickness at 850, due to the general increase in slope. Regarding accumulation that occurs after the deposition of the layer in question (851-999) perturbations that occur upstream of location 80 km cause a negative sensitivity because they increase the effect of dynamic thinning. Perturbations that occur downstream (> 80 km) or on the opposite section of the ice sheet (< 0 km) area cause a positive sensitivity, primarily because of the reduction of the surface gradient that we discussed previously.

3.2. Increased and Reduced SMB

We can now use our understanding of single-point perturbations to analyse variations in SMB with a broader spatial and temporal reach. Simulation SMB+ has the increased SMB curve between 150-200 kyr. At 155 kyr, after 5 kyr of anomalous SMB, layers above the 150 kyr isochrone (> 750) are thicker between 50-110 km due to the higher accumulation of the anomalous forcing (area 5, Fig. 4a). Older layers are not affected directly by an increase in SMB but only indirectly by changes in ice flow (area 6). Layers there are thinner because the higher SMB increases the elevation of the ice sheet between 50-110 km and steepens the surface gradient downstream. Velocities increase and more ice mass is lost, resulting in thinner layers. The mass that is lost from area 6, gets transported to area 3 and the layers there increase in thickness. This effect is stronger in younger layers that are closer to the surface and therefore subject to higher velocities (areas 2 and top of area 3).

The region from the left margin up to 50 km (areas 1 and 4) also shows an increase in layer thickness. This is explained by the increase in elevation at location 50-110 km, that decreases the slope upstream, thus reducing the velocities there. Smaller velocities mean less ice mass being lost and the layers remain thicker. It is notable that the entire section of the ice sheet of areas 1 and 4 is also affected with a positive thickness difference due to this change in surface slope at 50-110 km, even locations close to the left margin.

At the end of the simulation, at 200 kyr, the negative thickness anomaly between SMB+ and CTRL can be seen from 110 km all the way to the right ice sheet margin (area 3, Fig. 4b). At this point, the negative thickness anomaly from area 6 advects downstream to area 3 and overwhelms the initially positive signal. The same pattern is identified in the sensitivity simulation at 200 kyr (area 3, Fig. 2b). In both cases, the older layers, which became thinner as a result of dynamic thinning, advected their signal downstream

thus covering the whole section with a negative thickness difference. On the contrary, the younger layers (areas 2 and 5, Fig. 4b) show both an increase and a decrease of their thickness. The two signals coexist because these layers are subject to both increased thickness due to the direct SMB surplus and also thin more quickly due to the dynamic thinning created by younger layers. In addition, the thick layer anomaly is moved downstream by advection. The accumulation anomaly dominates where the cumulative effect of increased flow did not yet have enough time to act, which also explains the boundary between the two regions. It is important to note that the direct effect of the increase in SMB is much more prominent in the case of SMB+ than it was for the sensitivity simulation. In the latter one, the direct effect was only noticeable on the perturbed layer and did not really affect the general thickness of the layers. In the case of SMB+, the fact that SMB is increased for all layers > 750 combined with the increase in the magnitude of SMB anomaly, make the direct effect of SMB change a significant and influential factor for the final shape of the layers. As for areas 1 and 4 of the ice sheet, these preserve their positive thickness difference.

Given the changes that occur in layer thickness due to dynamic thinning, the elevation of the layers above the bedrock is also going to differ between SMB+ and CTRL. The result is a notable difference in the vertical age profiles (Fig. 5a), where the year 0 is defined as the surface layer. At 155 kyr there is a column of negative age difference between 50-110 km. The negative difference shows the presence of younger layers in SMB+ than in CTRL, at the same depth. This is directly related to the thickness anomaly (Fig. 4a). Since the layers of area 6 are thinner, they occupy deeper depths than in the CTRL experiment and thus have a smaller age difference. This can also be seen on the layer contours (Fig. 1d). The layers of SMB+ at the location where the increased anomaly occurs have sunk when compared to CTRL. Similarly, the section downstream of the 50-110 km column shows a positive age difference, because the thickness of the older layers is larger and thus they occupy shallower depths. The section upstream of the 50-110 km column shows an increase in the age difference, again due to the increase in layer thickness. The distribution of the age of the layers in the ice sheet and the corresponding depth at which each layer is found depends heavily on their thickness.

One anomaly in the age difference that does not have a direct correspondence in the perturbed layer thicknesses appears in the lower parts of the ice sheet. Figure 5a shows negative age difference located on the deeper layers of the ice sheet. This can be explained by the bedrock deformation in combination with the steep increase in isochrone age near the glacier bed. Since SMB+ has an ice sheet of a larger mass due to the increased SMB, the bedrock is subjected to greater weight. The ice sheet sinks due to the bedrock

deformation and the layers move downwards, indicating a negative age difference. The slight difference due to the sinking of the bedrock is mostly noticeable on the thinner bottom layers. The same difference on two simulations equivalent to SMB+ and CTRL but with a flat and non-deformable bedrock, shows that no age difference appears at the bottom of the ice sheet (Fig. 6a). With the exception of these very old layers near the bedrock, all other layers have similar age difference in both the solid and the deformable bedrock, indicating that the presence of bedrock deformation does not affect the final thickness of the layers significantly.

At 200 kyr (Fig. 5b), the section downstream of the 50-110 km column, for elevations lower than 850 m, has a negative age difference, following similar patterns as with area 3 in Fig. 4b. Thinner layers move downwards and thicker remain in higher elevation points. Near the bedrock, there is a larger presence of thin layers close to the bottom at 200 kyr when compared to 155 kyr, because dynamic thinning has acted for a longer period. This explains the reason the negative age difference effect appears much stronger. In the simulation without any bedrock deformation, there is no negative difference on the layers close to the bottom (Fig. 6b).

The differences in layer thickness between SMB– and CTRL at 200 kyr follow a pattern that is opposite to SMB+ (Fig. 7). Because of the reduction of SMB, the slope of the ice sheet downstream of 50-110 km decreases. This reduces the velocities and weakens the dynamic thinning. Old layers have increased thickness because of the reduced dynamic thinning. Younger layers experience both an increase and a decrease on their thickness according to whether the decrease in SMB or the reduced dynamic thinning prevails. When the reduction of SMB is stronger, the difference in thickness is negative, thus creating thinner layers.

The inverted pattern of layer thickness difference anomalies in SMB+ and SMB– indicate that even a relatively large SMB anomaly approximately causes a linear response, something that cannot necessarily be expected given the nonlinearity of Glen's flow law which governs dynamic thinning. We will test the linearity further in section 4.

3.3. Oscillatory SMB

The oscillating SMB anomalies in OSC start with the increased SMB distribution. After 155 kyr the SMB distribution completes its first oscillation. Layers 750-775 show one positive and one negative horizontal signal, indicating that the effect of the SMB oscillation is immediately recorded on the thickness of these layers (Fig. 8a). The information is primarily recorded downstream (area 2), but the region upstream (area

1) is also affected and the anomalies are consistent with the early phase of SMB+. The older layers (area 6) are only affected by dynamic thinning and to a lesser degree than SMB+ and SMB– (notice the difference in scale between the figures of OSC and SMB+ and SMB–) because, in the case of OSC, the average SMB anomaly is zero. The thickness difference of area 6 has both negative and positive signals. The negative signal is a result of the initial increased SMB that dynamically thins older layers as seen in SMB+. It gets transported downstream and affects also area 3. The positive signal of area 6 is a result of the following decreased SMB. Since the dynamic thinning occurs fast, it quickly affects all older layers between 50-110 km. These rapid changes in the thicknesses of the older layers are observed until the end of the simulation. Area 6 and the part of area 4 around the ice divide change sign according to the different phases of the oscillation. Area 6 shifts from a negative thickness difference when the SMB is increased at 197 kyr (Fig. 8b) to a positive one when the SMB is reduced at 200 kyr (Fig. 8c). These older layers are affected from the current signal of the SMB distribution and the response is fast. The signal alternates with the change in SMB and is always replaced with the current signal. The history of the oscillations is not present and no memory of previous signals appears. This fast reaction is in contrast with the downstream area 3. There, the anomalous ice thickness of the older layers preserves the same constant signal of both positive and negative thickness difference in both Fig. 8b and 8c. The fact that the signal does not change together with the oscillations shows a long term and slow effect of dynamic thinning. Lastly, at 200 kyr, all younger layers (area 2) show the transition betwen the oscillations and all 10 oscillations (50,000/5,000) are clearly visible as long horizontal signals. The thickness of the younger layer is affected by the direct change in SMB. These horizontal stripes are visible on the opposite side of the ice sheet (area 1) albeit with much less intensity.

In summary, the older layers for the two regions downstream and upstream of 750 km behave differently: On the upstream section (areas 6 and 4 around the ice divide), the thickness and age difference of the layers changes with the oscillations in SMB, while on the downstream (area 3) it remains constant. The periodic change of the total thickness difference for layers 1-500 at the upstream section (for example at 60 km, Fig. 9a) is of course explained because, after the initial negative offset dissapears, the mean of the oscillations is very close to 0, and thus the signal switches from positive to negative values. At the downstream section (for example at 180 km, Fig. 9b) the offset appears with a delay since its advecting from upstream, and the amplitude of the oscillations is not enough for the thickness difference to cross the 0 axis, thus remaining steadily on the negative for the whole examined period of 200 kyr.

3.4. Sliding

For the simulation SLID, sliding is activated between 170,991-171,000 years at 130 km and is an increased horizontal velocity of all the layers of the ice sheet by 10^{-6} m/s. The relatively short duration of 10 years was chosen analog to the small perturbation in SMB in the sensitivity simulation above. It is long enough to excite a measurable response. The location was chosen in one side of the ice sheet where horizontal ice flow is significant. Immediately after sliding is activated, two columns are formed due to this increase in velocity, one upstream with negative thickness difference between SLID and CTRL and one downstream with positive difference (Fig. 10a). The increased velocity of all layers enhances ice movement at 130 km and these two columns are formed, one that loses mass faster, making the layers thinner in SLID than CTRL, and one that receives this mass, making the layers thicker. At 200 kyr, this initial sliding effect does not affect newer layers, while in the old layers, the columns have advected downstream and are not vertical anymore (Fig. 10b). We have the appearance of three signals. An increased layer thickness difference at the lower right near the margin, a decreased layer thickness difference exactly on top and to the left, and again an increased thickness difference on the top and to the left. The first two are the columns of 171,000 years that have advected completely downstream. The third signal is created after 171,000 years and is a result of the two columns. Since the layer thickness of the column upstream of 130 km is decreased, the surfaces elevation decreases. Similarly downstream of 130 km, the surfaces elevation increases. This creates a flatter surface around 130 km, which reduces the long-term dynamic thinning, meaning that all layers upstream of this perturbation will have more mass. This explains the appearance of the positive third signal.

Since sliding increases ice velocity, its dynamical impact is identical to the increase in velocity due to changes in SMB. The emphasis of this analysis is to find a way to circumvent the effect of dynamic thinning by establishing a linear relation between SMB and layer thickness. As a result, we will not examine sliding further but instead we will isolate changes in SMB as the only factor that affects the stratigraphy of the ice sheet. Yet, at least we could confirm that the impact of sliding gives results that are well aligned and follow similar patterns to the effects of dynamic thinning that we have already covered.

4. TESTING THE QUALITY OF LINEAR APPROXIMATION

The analysis so far has shown how sustained SMB anomalies may be similar to the short perturbation, but also that non-linearities and asymmetries arise. This section will test the linearity of the three sustained SMB anomalies (SMB+, SMB– and OSC) further. Here we will use the linearized version of our model

as represented by the sensitivity matrix. The main question is if a linear superposition of the individual elements of the sensitivity matrix, scaled by the known amount of SMB, captures the thickness anomalies of the SMB+, SMB– and OSC cases, in spite of the known differences in time scales. The reconstructed RecSMB+, RecSMB– and RecOSC which will be shown in this section are not independent simulations, but linear summations of the 9,960 sensitivity simulations, scaled by the known values of SMB. The agreement between SMB+ - CTRL (ΔSMB+), SMB– - CTRL (ΔSMB–), OSC - CTRL (ΔOSC) and RecSMB+, RecSMB–, RecOSC respectively will be the objective of the following analysis.

We define as $\Delta M_{i_0,j_0}$ the deviation of SMB from CTRL, where i_0, j_0 are the horizontal location and layer where this deviation takes place. As shown in figure 1a, this occurs for i_0 between 72-77 (the six nodes corresponding to the 50-110 km area, with 10 km spacing) and, since it applies only for the years 150,000-200,000 (with 200 years per layer), j_0 is between 751-999. This change in SMB creates an ice sheet with a new set of layer thicknesses (SMB+, SMB-, OSC), whose thickness difference from CTRL is $\Delta d_{i,j}$, where i, j are the location and layer of the whole ice sheet. i varies between 0-133 (spatial model domain) while j between 1-999 (temporal domain). The relation between $\Delta M_{i_0,j_0}$ and $\Delta d_{i,j}$ is found from equation (1) and the Taylor series for multiple variables. By eliminating all second order derivatives, the series is written as:

$$\Delta d_{i,j} \approx \sum_{i_0,j_0} \left(\frac{\partial d_{i,j}}{\partial M_{i_0,j_0}} \Delta M_{i_0,j_0}\right) = \sum_{i_0,j_0} \left(\sigma_{i_0,j_0,i,j} \Delta M_{i_0,j_0}\right) \tag{2}$$

where the derivative is centered on CTRL, and it can thus be substituted with the sensitivity matrix σ. Note, that (2) is an approximation. The left-hand side of the approximation represents the thickness difference ΔSMB+, ΔSMB– and ΔOSC. The right-hand side represents a linear reconstruction RecSMB+, RecSMB– and RecOSC.

The anomalous layer thicknesses of RecSMB+ (Fig. 11a) are very similar to ΔSMB+ (Fig. 4b) and differences between the linearized and the full model are relatively small (Fig. 11b), indicating that the linearized reconstruction is a reasonably faithful representation of SMB+. Older layers downstream of the 50-110 km perturbation zone (area 3) show almost no mismatch, thus ΔSMB+ and RecSMB+ are almost identical.

The remaining differences can help to understand the shortcomings of the linearization. Newer layers downstream of the SMB perturbation at 50-110 km (area 2) show an inconsistency between ΔSMB+ and RecSMB+. The thickness difference is positive (Fig. 11a), and ΔSMB+ seems to have a stronger

positive difference on the upper right corner of the ice sheet and a weaker positive difference on the layers immediately below and to the left (areas 5 and 2, Fig. 11b). This is a result of the increase in surface slope. Because of the continuously increased SMB distribution, the SMB+ simulation creates a glacier of higher elevation than CTRL, increasing the surface slope and thus the effect of dynamic thinning. This is not captured by the linear superposition of sensitivity simulations where the individual SMB perturbations are fully independent, do not add up, and therefore only minimally alter the elevation. Since ΔSMB+ transports ice mass faster towards the right margin, the positive thickness difference is attenuated in comparison with RecSMB+. At the same time, since the same process pushes more mass downstream, a stronger positive signal appears on the upper right corner. In order to quantify the accuracy of the linearization, we define the deviation from linearization metric as:

$$\frac{\Sigma|RecSMB+| - \Sigma|\Delta SMB+|}{\Sigma|\Delta SMB+|} \cdot 100\% \tag{3}$$

The smaller the number, the more accurate the linearization. We exclude from the computation the grid points of the domain located near the margins, because these are prone to computational errors since they are very sensitive to small horizontal movements of the ice sheet. For the rest of the internal layers of the ice sheet, we get a total deviation of 5.22 %, meaning that around 95% of the SMB+ has been reconstructed via the linearization.

We can reach similar conclusions by looking at the results of RecSMB–. Comparison of figures 7 and 12a shows that the reconstructed thickness differences are similar in pattern. The difference between the two gives a quite accurate reconstruction for the older layers because the inconsistency between ΔSMB– and RecSMB– is very low (area 3, Fig. 12b). Since the SMB– simulation has a lower elevation than CTRL, it is expected that the dynamic thinning effect will be weaker in ΔSMB– than in RecSMB–, making the younger layers, which already have a negative thickness difference (Fig. 12a) have slower horizontal velocities for the case of ΔSMB- over CTRL. As a result of the weaker dynamics and horizontal movement, the negative thickness difference is enhanced, and this explains the negative sign in the comparison between ΔSMB- and CTRL (areas 5 and 2, Fig. 12b). In addition, since the negative signal moves less towards the right margin, it makes the layers of the upper right column appear thicker, thus explaining the positive sign at the upper part of area 2. The deviation from linearization of SMB– is found equal to 7.16 %.

Examining the case of RecOSC (Fig. 13a) we also find a similar pattern to ΔOSC (Fig. 8c). The difference between the two (Fig. 13b) indicates that there is no inconsistency in old layers (area 3) while the new layers

(areas 5 and 2) differ. Given the fact that during the oscillations the elevation of the ice sheet continuously alternates from higher to lower than in CTRL, we expect changes in dynamic thinning from stronger to weaker that are not represented in the sensitivity simulations and thus produce alternating mismatches. The deviation from linearization of the reconstruction is only 0.23 %, an order of magnitude smaller than the cases of RecSMB+ and RecSMB–. This smaller number shows that the linearization is an even better approximation for the case of OSC. Since OSC has no net SMB difference with CTRL, the change in elevation is very small, effects of differences in the strength of dynamic thinning are less impactful and thus a linearization can be considered more valid. This is the case even though the effect of dynamic thinning is fast and changes sign with every oscillation, as discussed above. However, since these anomalies are also short-lived, their long-term effect is negligible.

In conclusion, the reconstruction based on the linear sensitivities yields good results in these idealized cases. The main differences in layer thickness between SMB+, SMB–, OSC – CTRL were well captured on the reconstructed RecSMB+, RecSMB–, RecOSC respectively, indicating that extrapolating the linearized equation (2) gives an accurate approximation of the dynamical behavior of the ice sheet. This indicates that a linearized parameterization can largely account for the effect of ice flow. The primary reason for disagreements is sustained SMB that gives rise to surface elevation and slope changes and eventually dynamic thinning that is not accounted for by the linearization.

Given that, despite the differences, a linearization of the relationship between $\Delta M_{i_0,j_0}$ and $\Delta d_{i,j}$ yields defensible results, we will now briefly explore the possibility of solving an inverse problem and calculating the original SMB. The focus will be on the OSC simulation for two reasons: First because, as shown, the linearity is more accurate for the case of OSC, and secondly, the fact that SMB changes through time makes OSC a more realistic simulation. The main question is whether the full knowledge of the sensitivity matrix $\sigma_{i_0,j_0,i,j}$ and of the thickness difference $\Delta d_{i,j}$ are enough in order to calculate the anomalous SMB, and compare whether the calculation is the same as its actual value. Equation (2) can be rewritten in matrix notation:

$$\boldsymbol{D} = \boldsymbol{\sigma} \cdot \boldsymbol{M},$$

where $\boldsymbol{D}$ is a vector with dimensions $(i \cdot j)$ and contains the values $\Delta d_{i,j}$, $\boldsymbol{\sigma}$ is a matrix with dimensions $(i \cdot j) \times (i_0 \cdot j_0)$ and contains the values $\sigma_{i_0,j_0,i,j}$ and $\boldsymbol{M}$ is a vector with dimensions $(i_0 \cdot j_0)$ and contains

the values $\Delta M_{i_0,j_0}$. Since $\boldsymbol{\sigma}$ is known, and $\boldsymbol{D}$ is the thickness difference OSC - CTRL, we can transpose for $\boldsymbol{M}$, the only unknown:

$$\boldsymbol{M} = \boldsymbol{\sigma}^{-1}\boldsymbol{D} \tag{4}$$

As mentioned previously, i is between 0-133 and j between 1-999, while i_0 is between 72-77 (corresponding to 50-110 km) and j_0 between 751-999 (corresponding to 150-200 kyr). However, in order for $\boldsymbol{\sigma}$ to be invertible, it needs to be a square matrix and $i \cdot j$ needs to be the same as $i_0 \cdot j_0$. In order not to have an overdefined problem, with more equations than unknowns, we will solve the system of equations only for i between 72-77 and j between 751-999.

The comparison of SMB for the case of OSC at location 80 km between the reference (blue line) and the reconstruction (red line) shows that layers 900-999 are reconstructed well but the result for layers 750-900 does not have any physical meaning (Fig. 14). This means that we managed to reconstruct only the last 20,000 years. The presence of noise in the case of the older layers can be explained by examining the nature of the problem that we attempt to solve. The system of equations (4) is ill-conditioned, meaning that the solution is too sensitive to error, in this case computational machine error. By doing a simple inversion, this error propagates the solution to unnatural magnitudes, thus producing the noise-like result of figure 14. In order to filter out the noise, regularization methods are usually applied. Future work will examine an implementation of these methods and how much information about SMB reconstruction can be salvaged from isochronal layers.

5. DISCUSSION & CONCLUSION

The current study examined the influence that changes of SMB have on the internal layering of the ice sheet. Formulating a relation between these two factors is challenging because the effect of dynamic thinning depends on many factors including the thickness of the layers themselves, thus having a feedback mechanism where the layer thickness which is affected by the dynamics, also affects the dynamics. Previous works have described this relation with some notable assumptions, like the calculation of a strain rate based on a 1-D model (e.g. Leysinger Vieli and others, 2004; Siegert and Payne, 2004), or when horizontal flow is included, the ice sheet is on a steady state with a given velocity field (e.g. Baldwin and others, 2003; Waddington and others, 2007).

In this study, we used the isochronal numerical model by Born (2017) which does not require the ice sheet to be on a steady state. The surface of the ice sheet changes continuously with time, thus ice sheet dynamics and horizontal flow are always updated according to the SMB of the new layer. SMB affects layer thickness directly via the immediate change in precipitation and indirectly via changes in dynamic thinning. Direct changes of precipitation are more local and affect only the layer created at the time the precipitation occured, while changes in dynamic thinning have a strong influence in the whole ice sheet and also affect previous and following layers, making this the dominant factor. We examined a range of representative cases, with increased, reduced and seasonal SMB changes, and quantified the differences in layer thickness in each case. An increase in SMB increases the elevation and surface steepness, enhancing the dynamic thinning and creating thinner older layers.

In spite of the strongly non-linear response of dynamic thinning to changes in SMB, a linearized version of our model yielded a satisfactory representation of changes in layer thickness for a given alteration of SMB. The linearization was made by using a sensitivity matrix, a set of parameters calculated by forcing infinitesmal perturbations in the SMB of the model at every location and layer, and then quantifying the sensitivity of the layer thickness at each perturbation. Of the three tested cases, the linearization performed best for the simulation with oscillatory SMB anomaly. Because of the alternating nature of sinusoidal SMB, the net mass balance of the ice sheet at OSC remained closer to CTRL than for the cases of SMB+ and SMB– where the net mass balance was larger and smaller, respectively. Since the average shape of the ice sheet and the surface slope remained more similar, the dynamic behavior was also closer to CTRL, meaning that the linear approximation was more accurate since there was a smaller deviation from the original state of the ice sheet.

To isolate the effect of SMB on layer thickness, some aspects of the model were idealized. The horizontal velocities of the model are calculated using the shallow ice approximation and Glen's flow law. This means that the effect of dynamic thinning essentially depends on the slope of the surface. Vertical advection is not taken into consideration. In addition, since the aim was to focus on the influence of SMB alone, all other factors that could have affected the stratigraphy had to be neglected. Thus, the temperature of the ice sheet was taken equal to -5^oC and consequently the flow factor is constant. We argue that albeit the impact of temperature on ice deformation is substantial, uncertainty in this parameter is smaller than in SMB, in particular considering that the majority of deformation occurs near the base where temperatures are relatively stable. In addition, sliding was not taken directly into consideration for the linearization, but

its effect was examined and found to have a very similar dynamical behavior with changes in horizontal velocities due to SMB perturbations. As a result, incorporating sliding in the method is a possibility for future applications. Changes of state for the ice (freezing, melting etc.) are outside the scope of this research and do have a significant impact on layer stratigraphy (e.g. Leysinger-Vieli and others, 2018). Lastly, a transition to 3 dimensional flow and the presence of a non-flat bedrock are expected to add computational difficulties, but because of symmetricity in the horizontal dimensions we expect that our main findings are adaptable to 3D flow. Overall, within the limitations examined here, we find that the linear approximation is relatively accurate, in particular if carried out for cases where the changes in SMB are not too large.

The linearized approximation offers a new possibility for the reconstruction of past SMB. Layer thickness data from various sources, notably the radiostratigraphy archives of the ice sheets of Greenland and Antarctica (MacGregor and others, 2021) that not only cover layers thousands of years old, but are also quite dense with spatial information. By simplifying the relation between SMB and layer thickness and replacing the effect of ice flow with the sensitivity matrix, it becomes theoretically possible to solve for the SMB and get important reconstructions of the polar climate of the past and at different locations of the ice sheets. However, solving for SMB is not as simple as inverting the sensitivity matrix as was shown here in the idealized case of OSC, where by using the layer thickness difference and the 9,960 sensitivity simulations we got results that featured a lot of noise, an indication that the linear system of equations is ill-posed. This issue can be addressed by introducing regularization processes, which will be examined in future work.

REFERENCES

Baldwin D, Bamber J, Payne A and Layberry R (2003) Using internal layers from the Greenland ice sheet, identified from radio-echo sounding data, with numerical models. *Annals of Glaciology*, **37** (doi: 10.3189/172756403781815438)

Born A (2017) Tracer transport in an isochronal ice-sheet model. *Journal of Glaciology*, **63**(237), 2238 (doi: 10.1017/jog.2016.111)

Born A and Robinson A (2021) Modeling the Greenland englacial stratigraphy. *The Cryosphere*, **15**(9), 4539–4556 (doi: 10.5194/tc-15-4539-2021)

Clarke G and Marshall S (2002) Isotopic balance of the Greenland ice sheet: Modelled concentrations of water isotopes from 30,000 BP to present. *Quaternary Science Reviews*, **21**, 419–430 (doi: 10.1016/S0277-3791(01)00111-1)

564 Clarke G, Lhomme N and Marshall S (2005) Tracer transport in the Greenland ice sheet: Three-dimensional isotopic
565 stratigraphy. *Quaternary Science Reviews*, **24**, 155–171 (doi: 10.1016/j.quascirev.2004.08.021)

566 Cuffey K and Paterson W (2010) *The Physics of Glaciers*. Elsevier Science, ISBN 9780080919126

567 Cuffey KM and Clow GD (1997) Temperature, accumulation, and ice sheet elevation in central Greenland
568 through the last deglacial transition. *Journal of Geophysical Research: Oceans*, **102**(C12), 26383–26396 (doi:
569 https://doi.org/10.1029/96JC03981)

570 Dansgaard W and Johnsen SJ (1969) A flow model and a time scale for the ice core from Camp Century, Greenland.
571 *Journal of Glaciology*, **8**(53), 215223 (doi: 10.3189/S0022143000031208)

572 Goelles T, Grosfeld K and Lohmann G (2014) Semi-lagrangian transport of oxygen isotopes in polythermal ice
573 sheets: implementation and first results. *Geoscientific Model Development*, **7**(4), 1395–1408 (doi: 10.5194/gmd-7-
574 1395-2014)

575 Greve R (1997) Large-scale ice-sheet modelling as a means of dating deep ice cores in Greenland. *Journal of Glaciology*,
576 **43**(144), 307310 (doi: 10.3189/S0022143000003257)

577 Huybrechts P, Rybak O, Steinhage D and Pattyn F (2009) Past and present accumulation rate reconstruction along
578 the Dome Fuji-Kohnen radio-echo sounding profile, Dronning Maud Land, East Antarctica. *Annals of Glaciology*,
579 **50**, 112–120 (doi: 10.3189/172756409789097513)

580 Johnsen SJ, Dahl-Jensen D, Dansgaard W and Gundestrup N (1995) Greenland palaeotemperatures derived from
581 GRIP bore hole temperature and ice core isotope profiles. *Tellus B: Chemical and Physical Meteorology*, **47**(5),
582 624–629 (doi: 10.3402/tellusb.v47i5.16077)

583 Lasher GE, Axford Y, McFarlin JM, Kelly MA, Osterberg EC and Berkelhammer MB (2017) Holocene temperatures
584 and isotopes of precipitation in Northwest Greenland recorded in lacustrine organic materials. *Quaternary Science*
585 *Reviews*, **170**, 45–55, ISSN 0277-3791 (doi: https://doi.org/10.1016/j.quascirev.2017.06.016)

586 Le Meur E and Huybrechts P (1996) A comparison of different ways of dealing with isostasy: examples
587 from modelling the Antarctic ice sheet during the last glacial cycle. *Annals of Glaciology*, **23**, 309317 (doi:
588 10.3189/S0260305500013586)

589 Legarsky J and Gao X (2006) Internal layer tracing and agedepth relationship from the ice divide toward Jakobshavn,
590 Greenland. *IEEE Geoscience and Remote Sensing Letters*, **3**(4), 471–475 (doi: 10.1109/LGRS.2006.877749)

591 Leysinger-Vieli G, GJMC, Martn C, Hindmarsh and et al R (2018) Basal freeze-on generates complex ice-sheet
592 stratigraphy. *Nat Commun*, **9**, 4669 (doi: https://doi.org/10.1038/s41467-018-07083-3)

593 Leysinger Vieli GJMC, Siegert MJ and Payne AJ (2004) Reconstructing ice-sheet accumulation rates at ridge B,
594 East Antarctica. *Annals of Glaciology*, **39**, 326330 (doi: 10.3189/172756404781814519)

Leysinger Vieli GJMC, Hindmarsh RCA, Siegert MJ and Bo S (2011) Time-dependence of the spatial pattern of accumulation rate in East Antarctica deduced from isochronic radar layers using a 3-D numerical ice flow model. *Journal of Geophysical Research: Earth Surface*, **116**(F2) (doi: https://doi.org/10.1029/2010JF001785)

MacGregor JA and 9 others (2015) Radiostratigraphy and age structure of the Greenland ice sheet. *Journal of Geophysical Research: Earth Surface*, **120**(2), 212–241 (doi: https://doi.org/10.1002/2014JF003215)

MacGregor JA and 45 others (2021) The scientific legacy of NASAs Operation IceBridge. *Reviews of Geophysics*, **59**(2), e2020RG000712 (doi: https://doi.org/10.1029/2020RG000712), e2020RG000712 2020RG000712

Medley B and 12 others (2013) Airborne-radar and ice-core observations of annual snow accumulation over Thwaites Glacier, West Antarctica confirm the spatio-temporal variability of global and regional atmospheric models. *Geophysical Research Letters*, **40**, 3649–3654 (doi: 10.1002/grl.50706)

Mojtabavi S and 19 others (2020) A first chronology for the East Greenland ice-core project (EGRIP) over the Holocene and last glacial termination. *Climate of the Past*, **16**(6), 2359–2380 (doi: 10.5194/cp-16-2359-2020)

Nielsen LT, Karlsson NB and Hvidberg CS (2015) Large-scale reconstruction of accumulation rates in northern Greenland from radar data. *Annals of Glaciology*, **56**(70), 7078 (doi: 10.3189/2015AoG70A062)

Noon PE, Leng MJ and Jones VJ (2003) Oxygen-isotope (d18O) evidence of Holocene hydrological changes at Signy Island, maritime Antarctica. *The Holocene*, **13**(2), 251–263 (doi: 10.1191/0959683603hl611rp)

Nye JF (1963) Correction factor for accumulation measured by the thickness of the annual layers in an ice sheet. *Journal of Glaciology*, **4**(36), 785788 (doi: 10.3189/S0022143000028367)

Pinglot JF, Hagen JO, Melvold K, Eiken T and Vincent C (2001) A mean net accumulation pattern derived from radioactive layers and radar soundings on Austfonna, Nordaustlandet, Svalbard. *Journal of Glaciology*, **47**(159), 555566 (doi: 10.3189/172756501781831800)

Rybak O and Huybrechts P (2003) A comparison of Eulerian and Lagrangian methods for dating in numerical ice-sheet models. *Annals of Glaciology - ANN GLACIOL*, **37** (doi: 10.3189/172756403781815393)

Siegert M and Payne A (2004) Past rates of accumulation in central West Antarctica. *Geophysical Research Letters*, **31** (doi: 10.1029/2004GL020290)

Spikes VB, Hamilton GS, Arcone SA, Kaspari S and Mayewski PA (2004) Variability in accumulation rates from GPR profiling on the West Antarctic plateau. *Annals of Glaciology*, **39**, 238244 (doi: 10.3189/172756404781814393)

Sutter J, Fischer H and Eisen O (2021) Investigating the internal structure of the Antarctic ice sheet: the utility of isochrones for spatiotemporal ice-sheet model calibration. *The Cryosphere*, **15**(8), 3839–3860 (doi: 10.5194/tc-15-3839-2021)

Tarasov L and Peltier W (2003) Greenland glacial history, borehole constraints, and Eemian extent. *J. Geophys. Res*, **108** (doi: 10.1029/2001JB001731)

627 Waddington ED, Neumann TA, Koutnik MR, Marshall HP and Morse DL (2007) Inference of accumulation-
628 rate patterns from deep layers in glaciers and ice sheets. *Journal of Glaciology*, **53**(183), 694712 (doi:
629 10.3189/002214307784409351)

630 Winter A, Steinhage D, Creyts TT, Kleiner T and Eisen O (2019) Age stratigraphy in the East Antarctic Ice Sheet
631 inferred from radio-echo sounding horizons. *Earth System Science Data*, **11**(3), 1069–1081 (doi: 10.5194/essd-11-
632 1069-2019)

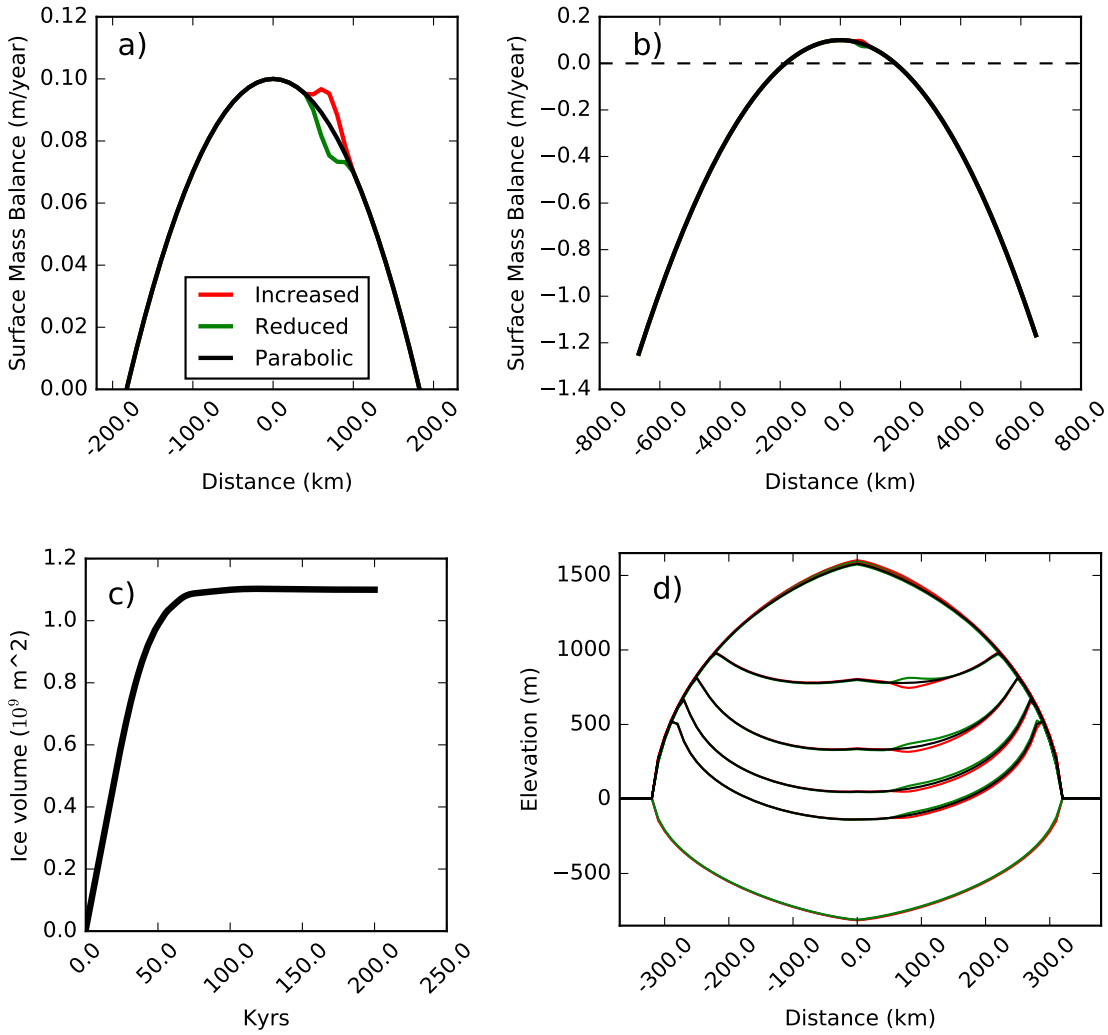

Fig. 1. (a) **Increased, reduced and parabolic distribution of surface mass balance.** All simulations use the **parabolic** SMB between 0-150,000 years. After that, between 150,000-200,000 years, CTRL continues with the **parabolic**, but SMB+, SMB– with the **increased** and **reduced** SMB distributions respectively. OSC oscillates between the two with a period of 5,000 years. (b) Same as (a) but with the full domain of the SMB, including the melting regions. (c) Evolution of total ice volume in CTRL (d) The isochronal layers at 160, 170, 180, 190 and 200 (same as the surface) kyr for CTRL, SMB+ and SMB- in the ice sheet's domain at 200 kyr.

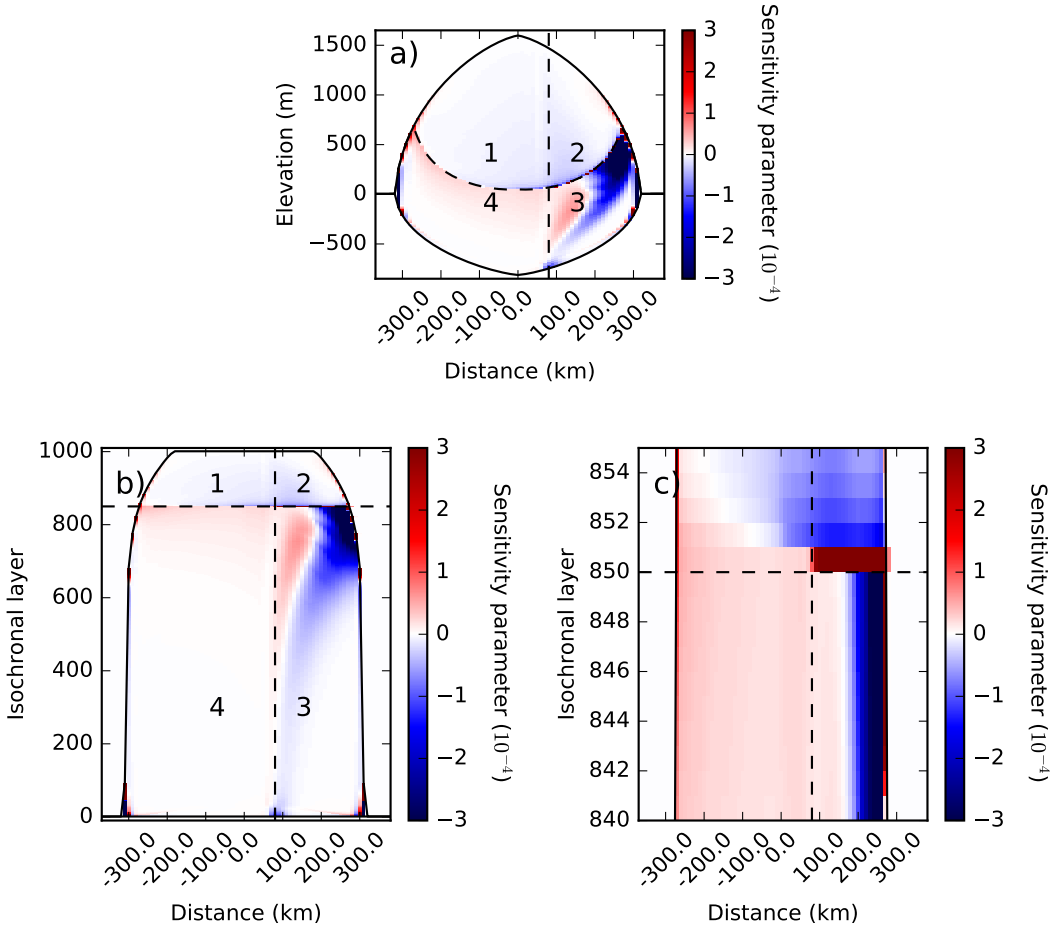

Fig. 2. (a) Sensitivity parameter of all regions of the ice sheet, as affected by a perturbation at location 80 km and layer 850 (point where dashed lines intersect) at 200 kyr. The domain is split into four areas 1,2,3 and 4 in order to better explain the phenomena observed. (b) Same as (a) but the y-axis shows each one of the isochronal layers instead of the elevation. (c) same as (b) but zoomed around the perturbed layer 850.

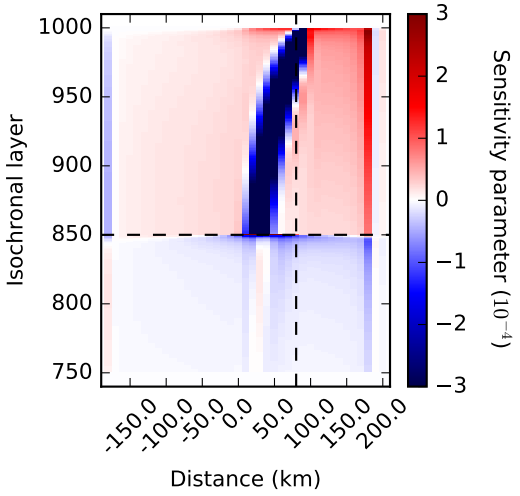

Fig. 3. Sensitivity parameter at 80 km and layer 850 (point where dashed lines intersect) as affected by perturbation in all regions of the ice sheet. Layers 1-750 are not shown because no perturbation of the SMB is applied for those layers.

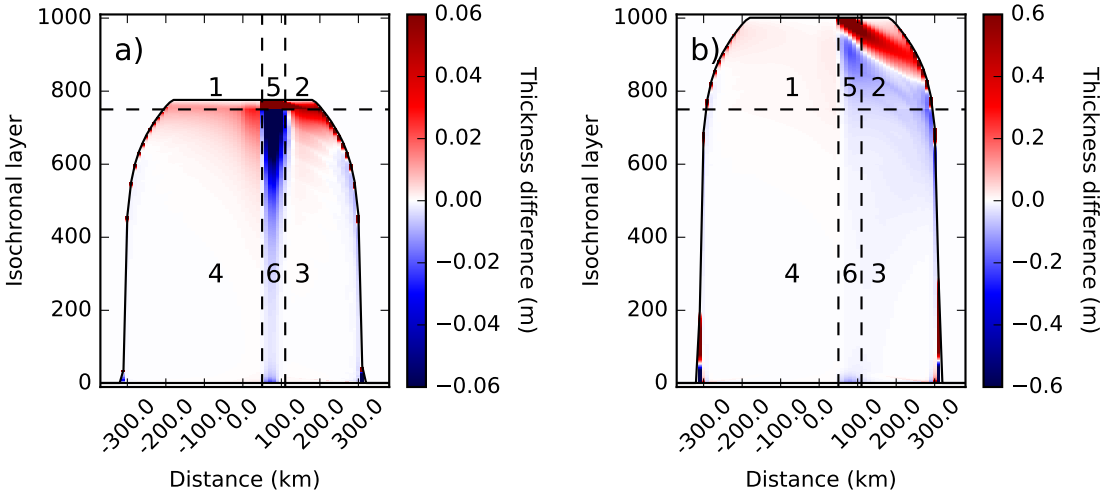

Fig. 4. Simulations **SMB+ - CTRL**. The increased SMB applies inside the area marked by the two vertical dashed lines (50-110 km), and between the dashed horizontal and the ice surface (layer 750-last layer). Thickness difference at (a) 155 kyr (b) 200 kyr.

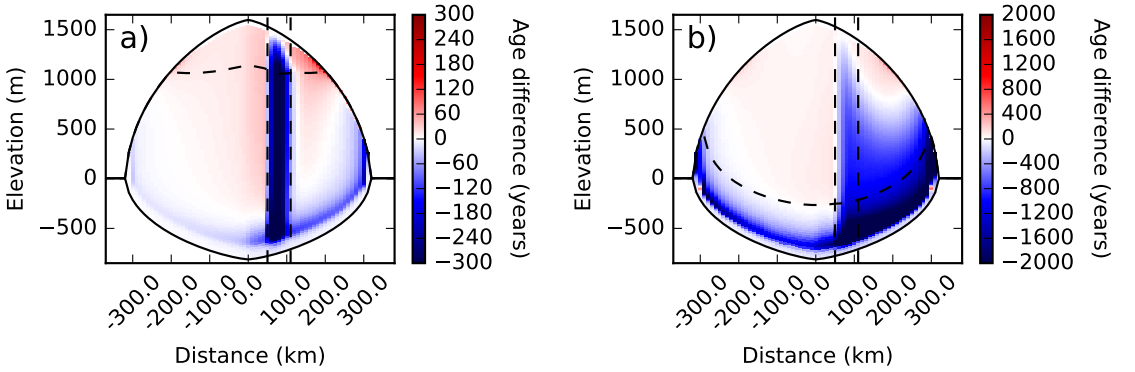

Fig. 5. Simulations **SMB+ - CTRL**. The increased SMB applies inside the area marked by the two vertical dashed lines (50-110 km), and between the dashed horizontal and the ice surface (layer 750-last layer). Age difference at (a) 155 kyr (b) 200 kyr.

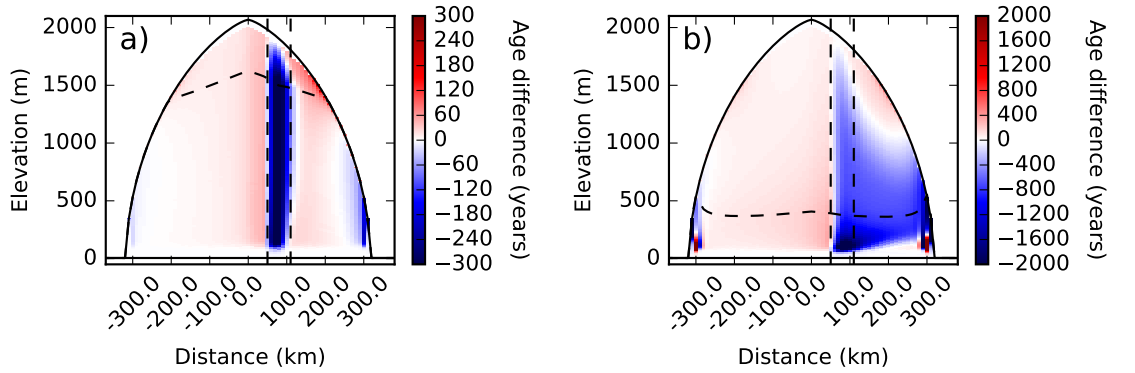

Fig. 6. Simulations **SMB+ - CTRL** but with no bedrock deformation. The increased SMB applies inside the area marked by the two vertical dashed lines (50-110 km), and between the dashed horizontal and the ice surface (layer 750-last layer). Age difference at (a) 155 kyr (b) 200 kyr.

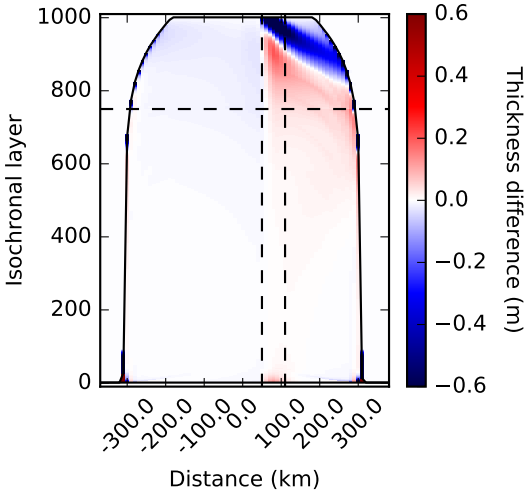

Fig. 7. Simulations **SMB– - CTRL** The reduced SMB applies inside the area marked by the two vertical dashed lines (50-110 km), and between the dashed horizontal and the ice surface (layer 750-last layer). Thickness difference at 200 kyr.

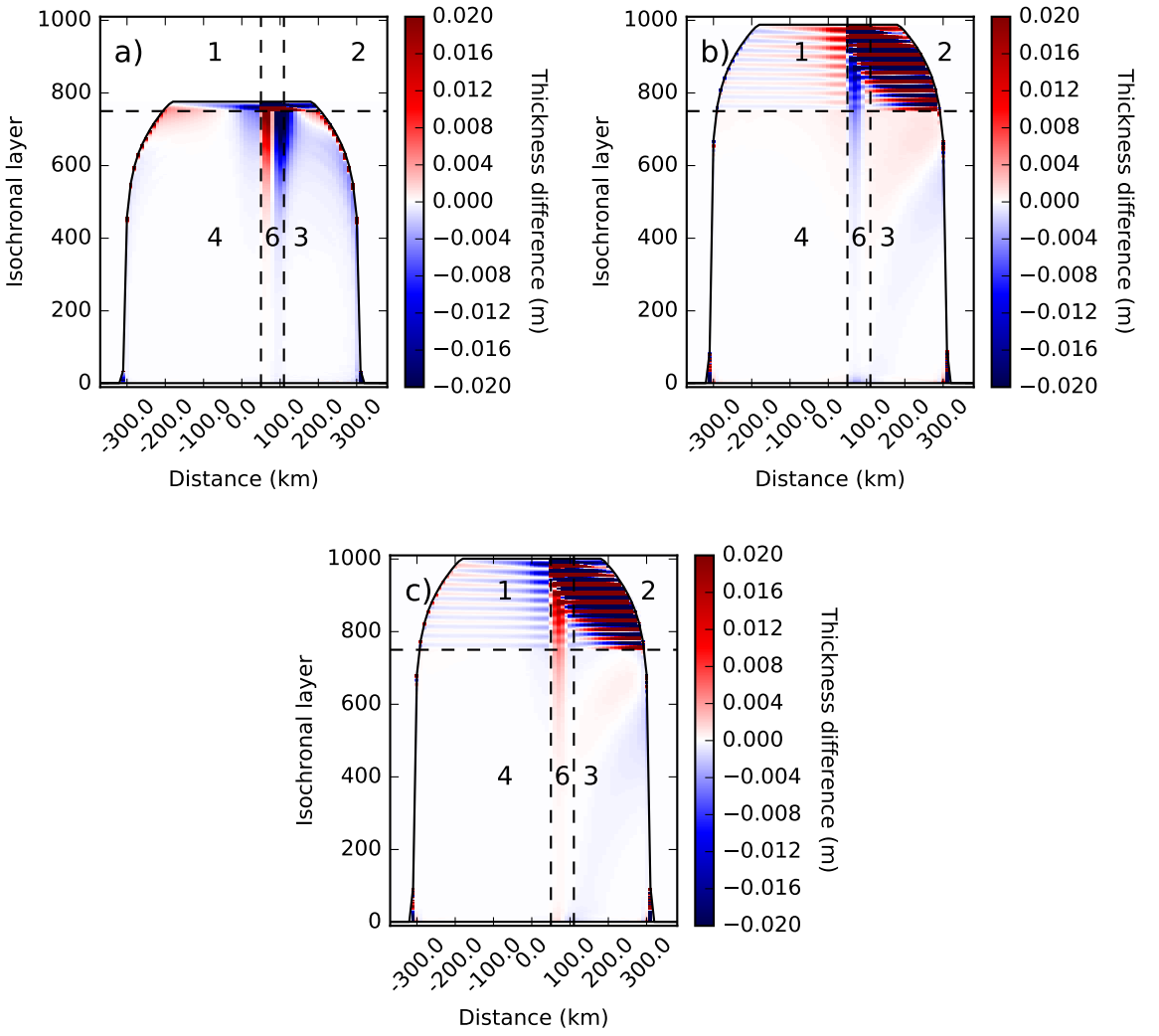

Fig. 8. Simulations **OSC - CTRL**. The oscillatory SMB applies inside the area marked by the two vertical dashed lines (50-110 km), and between the dashed horizontal and the ice surface (layer 750-last layer). Thickness difference at (a) 155 kyr (after one full oscillation) (b) 197 kyr (c) 200 kyr.

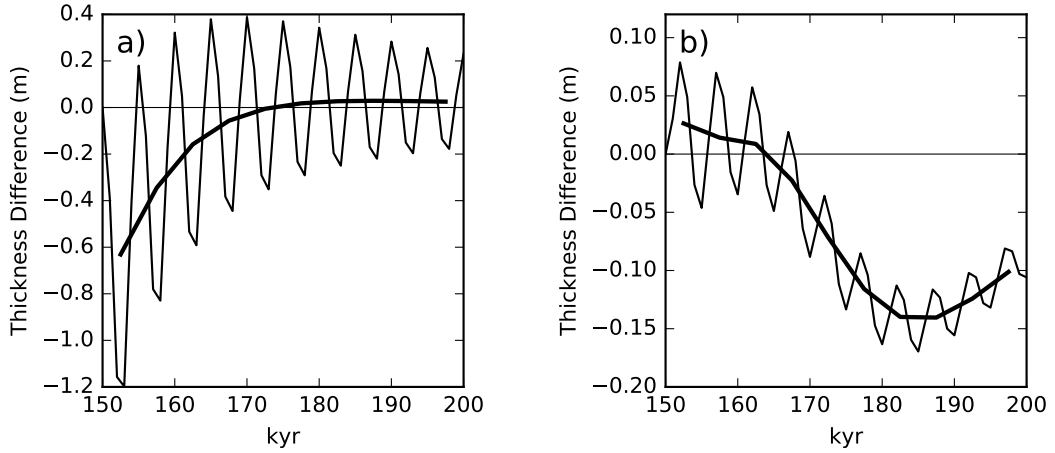

Fig. 9. Simulations **OSC - CTRL**. Evolution of the total thickness difference of all layers 1-500 at (a) 60 km (b) 180 km. The thick line is a 5-point running average.

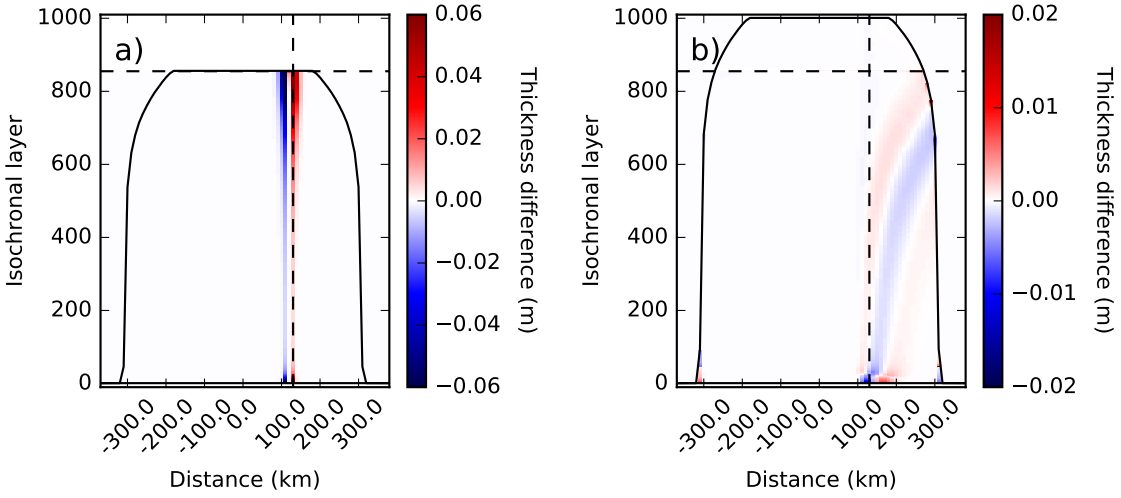

Fig. 10. Simulations **SLID - CTRL**. The sliding applies at 170,991-171,000 years, at 130 km (point where dashed lines intersect). Thickness difference at (a) 171 kyr (b) 200 kyr.

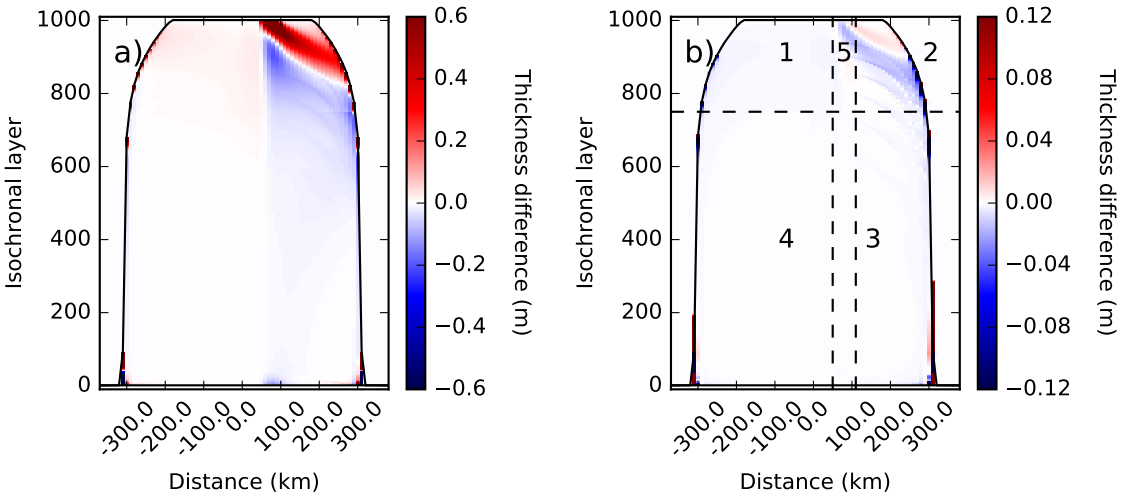

Fig. 11. RecSMB+ (a) Thickness difference at 200 kyr (b) The difference between figures 4b - 11a. Note that the scale is 5 times smaller than 11a.

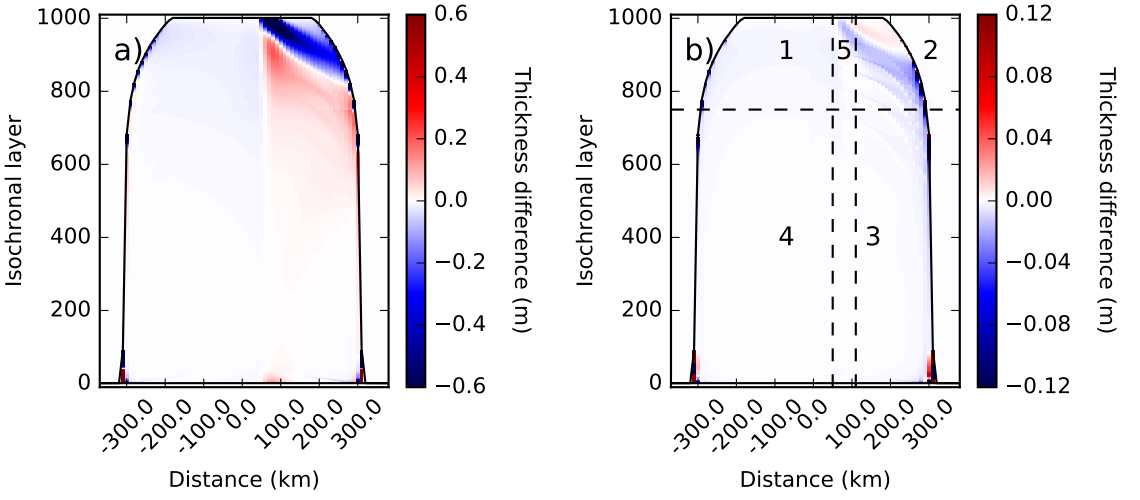

Fig. 12. RecSMB- (a) Thickness difference at 200 kyr (b) The difference between figures 7 - 12a. Note that the scale is 5 times smaller than 12a.

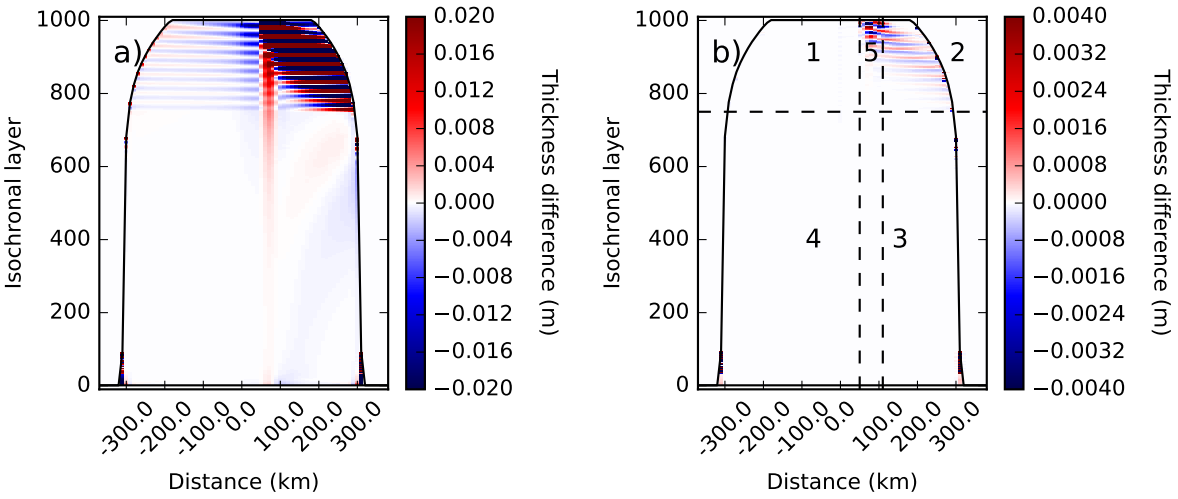

Fig. 13. RecOSC (a) Thickness difference at 200 kyr (b) The difference between figures 8c - 13a. Note that the scale is 30 times smaller than 11b, indicating a much smaller incosistency than RecSMB+ and RecSMB–.

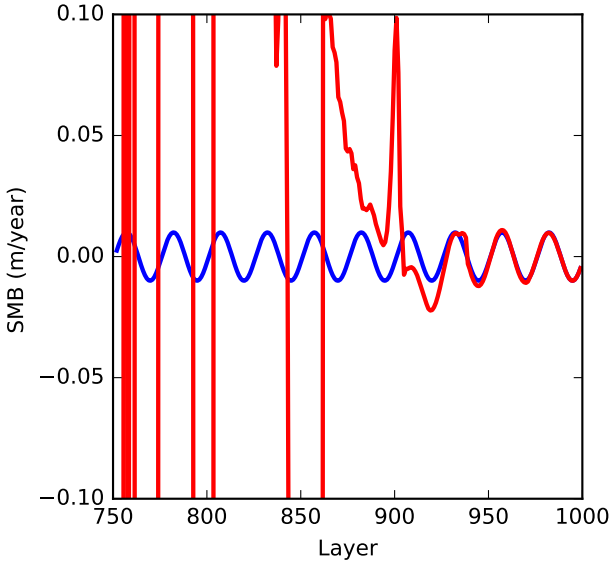

Fig. 14. Comparison between the actual SMB difference at location 80 km (blue line) and the calculated one from the inverse solution (red line) (Equation (4)), for the cases of OSC - CTRL.

Chapter 5

Discussion and future perspectives

This thesis proposes a new inversion method for reconstructing surface mass balance (SMB) by only considering the internal layer thickness of an ice sheet. Unlike the very commonly used strain rate by *Dansgaard and Johnsen* (1969), the method proposed in this thesis takes into consideration horizontal flow as a significant factor for determining the relation between SMB and layer thickness. The inversion method reconstructs SMB directly, and not through a process of data assimilation of trying to fit englacial layers to data, by defining a balance velocity field (*Baldwin et al.*, 2003). In that regard, the method has a lot of similarities with the inversion method proposed by *Waddington et al.* (2007). However, unlike this reconstruction, ours does not require a steady state ice sheet. This is achieved by using an isochronal numerical model introduced by *Born* (2017).

Of course, the method presented here has several simplifications. The isochronal layer model represents only a single cross-section of an ice sheet so that flow at right angles is neglected. While this should not be a problem when reconstructing target simulations, since these are also 2D, it definitely is a problem when applying the method on the real GrIS, which has ice flow in both meridional and zonal directions. The choice of section through the summit of the GrIS is made to minimize the effect of this simplification. A second simplification is that velocities are calculated through the shallow ice approximation, thus neglecting longitudinal stresses. In addition, the temperature was also taken as a constant everywhere, thus neglecting the implications that temperature has on ice viscosity and simplifying the properties of ice flow. The melt rate in regions with negative SMB is also taken as constant, even though its value affects layer thickness since it determines the maximum horizontal extent of the ice sheet. Other factors that were disregarded include basal sliding, ice deformation and processes of freezing and melting.

Although the problem oversimplifies a lot of aspects of the ice sheet, it also overcomplicates others. In the inversion method presented here all locations and layers were considered to have an unknown amount of SMB, and the corresponding SMBs were completely independant from each other. This is not true for the real GrIS. Precipitation rates can be approximated from $\delta^{18}O$ measurements and temperature variability (*Johnsen et al.*, 1995; *Witt and Schumann*, 2005). Interpolating between data at different ice core locations can also provide an important clue for the spatial pattern of SMB distribution. Extrapolation of these patterns could help with poorly known melt rates near the margins. By incoprorating this a priori knowledge, the degrees of freedom of

the expected SMB are going to decrease. The inversion as it was implemented here did not use any additional information, and the SMB of all locations at all times was taken as an unknown, thus increasing the complexity of the linear system of equations to the maximum possible number of unknowns for the present ice sheet. This was done in order to preserve the generalization and the flexibility of the solution without having the limitation of additional knowledge at specific ice sheets and locations, but an implementation of the method on the GrIS with the aim to accurately reconstruct the SMB of the past would be greatly benefited by additional data that can help push the solution to the correct result.

The important thing is that despite the simplifications and the lack of additional data that might facilitate the method, the reconstructed SMB of the GrIS at 72.5^o N, 38.3^o W showed a good agreement with the data from the GISP2 ice core (Paper II). Future work should focus on making the simulated ice sheet more complex in order to simulate the GrIS more realistically. Some steps to improve upon these simplifications have already been made. The model has recently been updated to a 3D version that represents the isochrones of the entire GrIS (*Born and Robinson*, 2021). Also, the reconstructed solution could be optimized by using additional constraints in the model. By limiting the degrees of freedom of the SMB in order to mimic the real characteristics of the GrIS, a more accurate solution might be found.

Bibliography

Amante, C., and B. Eakins (2009), ETOPO1 1 Arc-Minute Global Relief Model: procedures, data sources and analysis, doi:10.7289/V5C8276M. 6

Baldwin, D., J. Bamber, A. Payne, and R. Layberry (2003), Using internal layers from the Greenland ice sheet, identified from radio-echo sounding data, with numerical models, *Annals of Glaciology*, *37*, doi:10.3189/172756403781815438. 2, 91

Bales, R. C., E. Mosley-Thompson, and J. R. McConnell (2001), Variability of accumulation in northwest Greenland over the past 250 years, *Geophysical Research Letters*, *28*(14), 2679–2682, doi:https://doi.org/10.1029/2000GL011634. 2

Bjorck, A. (1991), Algorithms for linear least squares problems, doi:10.1007/978-3-642-76717-3-3. 11, 12

Born, A. (2017), Tracer transport in an isochronal ice-sheet model, *Journal of Glaciology*, *63*(237), 22–38, doi:10.1017/jog.2016.111. 3, 5, 7, 91

Born, A., and A. Robinson (2021), Modeling the Greenland englacial stratigraphy, *The Cryosphere Discussions*, *2020*, 1–27, doi:10.5194/tc-2020-355. 92

Brufati, T. E., S. Oliveira, and A. Bassrei (2016), Conjugate gradient method for the solution of inverse problems: Application in linear seismic tomography, *Trends in Computational and Applied Mathematics*, *16*(3), 185, doi:10.5540/tema.2015.016.03.0185. 12

Calvetti, D., S. Morigi, L. Reichel, and F. Sgallari (2000), Tikhonov regularization and the L-curve for large discrete ill-posed problems, *Journal of Computational and Applied Mathematics*, *123*(1), 423–446, doi:https://doi.org/10.1016/S0377-0427(00)00414-3, numerical Analysis 2000. Vol. III: Linear Algebra. 11

Calvetti, D., L. Reichel, and A. Shuibi (2003), Enriched Krylov subspace methods for ill-posed problems, *Linear Algebra and its Applications*, *362*, 257–273. 10, 12

Cuffey, K. M., and G. D. Clow (1997), Temperature, accumulation, and ice sheet elevation in central Greenland through the last deglacial transition, *Journal of Geophysical Research: Oceans*, *102*(C12), 26,383–26,396, doi:https://doi.org/10.1029/96JC03981. 2

Dansgaard, W., and S. J. Johnsen (1969), A flow model and a time scale for the ice core from Camp Century, Greenland, *Journal of Glaciology*, *8*(53), 215–223, doi:10.3189/S0022143000031208. 1, 2, 91

Diamond, M. (1960), Air temperature and precipitation on the Greenland ice sheet, *Journal of Glaciology*, *3*(27), 558–567, doi:10.3189/S0022143000023674. 1

Donatelli, M., and L. Reichel (2014), Square smoothing regularization matrices with accurate boundary conditions, *Journal of Computational and Applied Mathematics*, *272*, 334–349, doi:https://doi.org/10.1016/j.cam.2013.08.015. 10, 11

Fahnestock, M., W. Abdalati, S. Luo, and S. Gogineni (2001), Internal layer tracing and age-depth-accumulation relationships for the northern Greenland ice sheet, *Journal of Geophysical Research: Atmospheres*, *106*(D24), 33,789–33,797, doi:https://doi.org/10.1029/2001JD900200. 2

Golub, G. (1965), Numerical methods for solving linear least squares problems, *Numerische Mathematik*, *7*, 206–216. 11

Golub, G., and C. Reinsch (1970), Singular value decomposition and least squares solutions., *Numer. Math.*, *14*, 403–420, doi:https://doi.org/10.1007/BF02163027. 12

Hanke, M., and C. Groetsch (1998), Nonstationary iterated Tikhonov regularization, *Journal of Optimization Theory and Applications*, *98*, 37–53, doi:10.1023/A:1022680629327. 10

Hansen, P. C. (1990), Truncated singular value decomposition solutions to discrete ill-posed problems with ill-determined numerical rank, *SIAM Journal on Scientific and Statistical Computing*, *11*(3), 503–518, doi:10.1137/0911028. 12

Hansen, P. C., and D. O'leary (1993), The use of the L-curve in the regularization of discrete ill-posed problems, *SIAM J. Sci. Comput.*, *14*, 1487–1503, doi:10.1137/0914086. 11

Heath, M. T. (1974), *The Numerical Solution of Ill-Conditioned Systems of Linear Equations*, Oak Ridge National Laboratory, Central Research Library, Tennessee, operated by Union Carbide Corporations for the U.S. Atomic Energy Commission. 11, 12

Hochstenbach, M., and L. Reichel (2010), *An iterative method for Tikhonov regularization with a general linear regularization operator*, CASA-report, Technische Universiteit Eindhoven. 11

Huybrechts, P., O. Rybak, D. Steinhage, and F. Pattyn (2009), Past and present accumulation rate reconstruction along the Dome Fuji-Kohnen radio-echo sounding profile, Dronning Maud Land, East Antarctica, *Annals of Glaciology*, *50*, 112–120, doi:10.3189/172756409789097513. 2

Jacobel, R. W., and B. C. Welch (2005), A time marker at 17.5 kyr bp detected throughout west antarctica, *Annals of Glaciology*, *41*, 47–51, doi:10.3189/172756405781813348. 2

Johnsen, S. J., D. Dahl-Jensen, W. Dansgaard, and N. Gundestrup (1995), Greenland palaeotemperatures derived from grip bore hole temperature and ice core isotope profiles, *Tellus B: Chemical and Physical Meteorology*, *47*(5), 624–629, doi:10.3402/tellusb.v47i5.16077. 91

Kilmer, M. E., and D. P. O'Leary. (2001), Choosing regularization parameters in iterative methods for ill-posed problems, *SIAM Journal on Matrix Analysis and Applications*, *22*(4), 1204–1221, doi:10.1137/S0895479899345960. 11

Koutnik, M. R., E. D. Waddington, and D. P. Winebrenner (2009), A method to infer past surface mass balance and topography from internal layers in martian polar layered deposits, *Icarus*, *204*(2), 458–470, doi:https://doi.org/10.1016/j.icarus.2009.06.019. 2

Le Meur, E., and P. Huybrechts (1996), A comparison of different ways of dealing with isostasy: examples from modelling the Antarctic ice sheet during the last glacial cycle, *Annals of Glaciology*, *23*, 309–317, doi:10.3189/S0260305500013586. 6

Legarsky, J., and X. Gao (2006), Internal layer tracing and age–depth relationship from the ice divide toward Jakobshavn, Greenland, *IEEE Geoscience and Remote Sensing Letters*, *3*(4), 471–475, doi:10.1109/LGRS.2006.877749. 1

Leysinger Vieli, G. J.-M. C., M. J. Siegert, and A. J. Payne (2004), Reconstructing ice-sheet accumulation rates at ridge B, East Antarctica, *Annals of Glaciology*, *39*, 326–330, doi:10.3189/172756404781814519. 2

Leysinger Vieli, G. J.-M. C., R. C. A. Hindmarsh, M. J. Siegert, and S. Bo (2011), Time-dependence of the spatial pattern of accumulation rate in East Antarctica deduced from isochronic radar layers using a 3-D numerical ice flow model, *Journal of Geophysical Research: Earth Surface*, *116*(F2), doi:https://doi.org/10.1029/2010JF001785. 2

MacGregor, J. A., M. A. Fahnestock, G. A. Catania, J. D. Paden, S. Prasad Gogineni, S. K. Young, S. C. Rybarski, A. N. Mabrey, B. M. Wagman, and M. Morlighem (2015), Radiostratigraphy and age structure of the Greenland ice sheet, *Journal of Geophysical Research: Earth Surface*, *120*(2), 212–241, doi:https://doi.org/10.1002/2014JF003215. 1

MacGregor, J. A., L. N. Boisvert, B. Medley, A. A. Petty, J. P. Harbeck, R. E. Bell, J. B. Blair, E. Blanchard-Wrigglesworth, E. M. Buckley, M. S. Christoffersen, J. R. Cochran, B. M. Csathó, E. L. De Marco, R. T. Dominguez, M. A. Fahnestock, S. L. Farrell, S. P. Gogineni, J. S. Greenbaum, C. M. Hansen, M. A. Hofton, J. W. Holt, K. C. Jezek, L. S. Koenig, N. T. Kurtz, R. Kwok, C. F. Larsen, C. J. Leuschen, C. D. Locke, S. S. Manizade, S. Martin, T. A. Neumann, S. M. Nowicki, J. D. Paden, J. A. Richter-Menge, E. J. Rignot, F. Rodríguez-Morales, M. R. Siegfried, B. E. Smith, J. G. Sonntag, M. Studinger, K. J. Tinto, M. Truffer, T. P. Wagner, J. E. Woods, D. A. Young, and J. K. Yungel (2021), The scientific legacy of NASA's Operation IceBridge, *Reviews of Geophysics*, *59*(2), e2020RG000,712, doi:https://doi.org/10.1029/2020RG000712, e2020RG000712 2020RG000712. 6

Marshall, S., and K. Cuffey (2000), Peregrinations of the Greenland ice sheet divide in the last glacial cycle: Implications for central Greenland ice cores, *Earth and Planetary Science Letters*, *179*, 73–90, doi:10.1016/S0012-821X(00)00108-4. 1

Mojtabavi, S., F. Wilhelms, E. Cook, S. M. Davies, G. Sinnl, M. Skov Jensen, D. Dahl-Jensen, A. Svensson, B. M. Vinther, S. Kipfstuhl, G. Jones, N. B. Karlsson, S. H. Faria, V. Gkinis, H. A. Kjær, T. Erhardt, S. M. P. Berben, K. H. Nisancioglu, I. Koldtoft,

and S. O. Rasmussen (2020), A first chronology for the East Greenland ice-core project (EGRIP) over the Holocene and last glacial termination, *Climate of the Past*, *16*(6), 2359–2380, doi:10.5194/cp-16-2359-2020. 1

Morse, D. L., E. D. Waddington, H.-P. Marshall, T. A. Neumann, E. J. Steig, J. E. Dibb, D. P. Winebrenner, and R. J. Arthern (1999), Accumulation rate measurements at Taylor Dome, East Antarctica: Techniques and strategies for mass balance measurements in polar environments, *Geografiska Annaler: Series A, Physical Geography*, *81*(4), 683–694, doi:https://doi.org/10.1111/1468-0459.00106. 1

Nereson, N. A., C. F. Raymond, R. Jacobel, and E. D. Waddington (2000), The accumulation pattern across Siple Dome, West Antarctica, inferred from radar-detected internal layers, *Journal of Glaciology*, *46*(152), 75–87, doi:10.3189/172756500781833449. 2

Nielsen, L. T., N. B. Karlsson, and C. S. Hvidberg (2015), Large-scale reconstruction of accumulation rates in northern Greenland from radar data, *Annals of Glaciology*, *56*(70), 70–78, doi:10.3189/2015AoG70A062. 2

Nye, J. F. (1963), Correction factor for accumulation measured by the thickness of the annual layers in an ice sheet, *Journal of Glaciology*, *4*(36), 785–788, doi:10.3189/S0022143000028367. 1

Paterson, W. S. B., and E. D. Waddington (1984), Past precipitation rates derived from ice core measurements: Methods and data analysis, *Reviews of Geophysics*, *22*(2), 123–130, doi:https://doi.org/10.1029/RG022i002p00123. 2

Pinglot, J. F., J. O. Hagen, K. Melvold, T. Eiken, and C. Vincent (2001), A mean net accumulation pattern derived from radioactive layers and radar soundings on Austfonna, Nordaustlandet, Svalbard, *Journal of Glaciology*, *47*(159), 555–566, doi:10.3189/172756501781831800. 1

Pälli, A., J. C. Kohler, E. Isaksson, J. C. Moore, J. F. Pinglot, V. A. Pohjola, and H. Samuelsson (2002), Spatial and temporal variability of snow accumulation using ground-penetrating radar and ice cores on a Svalbard glacier, *Journal of Glaciology*, *48*(162), 417–424, doi:10.3189/172756502781831205. 1

Reichel, L., F. Sgallari, and Q. Ye (2012), Tikhonov regularization based on generalized Krylov subspace methods, *Applied Numerical Mathematics - APPL NUMER MATH*, *62*, doi:10.1016/j.apnum.2010.10.002. 10, 11

Riley, J. D. (1955), Solving systems of linear equations with a positive definite, symmetric, but possibly ill-conditioned matrix, *Mathematical Tables and Other Aids to Computation*, *9*(51), 96–101. 10, 11

Siegert, M., and A. Payne (2004), Past rates of accumulation in central West Antarctica, *Geophysical Research Letters*, *31*, doi:10.1029/2004GL020290. 2

Siegert, M. J., R. C. A. Hindmarsh, and G. S. Hamilton (2003), Evidence for a large surface ablation zone in central East Antarctica during the last Ice Age, *Quaternary Research*, *59*(1), 114–121, doi:10.1016/S0033-5894(02)00014-5. 2

Spigler, R. (2020), On the numerical solution of ill conditioned linear systems by regularization and iteration, *Numerical Linear Algebra with Applications*, *28*, doi:10.1002/nla.2335. 11

Spikes, V. B., G. S. Hamilton, S. A. Arcone, S. Kaspari, and P. A. Mayewski (2004), Variability in accumulation rates from GPR profiling on the West Antarctic plateau, *Annals of Glaciology*, *39*, 238–244, doi:10.3189/172756404781814393. 1

Steen-Larsen, H., E. Waddington, and M. Koutnik (2010), Formulating an inverse problem to infer the accumulation-rate pattern from deep internal layering in an ice sheet using a Monte Carlo approach, *Journal of Glaciology*, *56*, 318–332, doi:10.3189/002214310791968476. 2

Stewart, G. W. (1993), On the early history of the singular value decomposition, *SIAM Rev.*, *35*, 551–566. 12

Ternovski, V. V., M. M. Khapaev, and A. S. Grushicin (2015), Ill-posed algebraic systems with noise data, *Applied and Computational Mathematics*, *4*(3), 220–224, doi:10.11648/j.acm.20150403.25. 10

Twomey, S. (1963), On the numerical solution of Fredholm integral equations of the first kind by the inversion of the linear system produced by quadrature, *J. ACM*, *10*(1), 97–101, doi:10.1145/321150.321157. 11

Varah, J. M. (1973), On the numerical solution of ill-conditioned linear systems with applications to ill-posed problems, *SIAM Journal on Numerical Analysis*, *10*(2), 257–267, doi:10.1137/0710025. 12

Vaughan, D., H. Corr, and C. e. a. Doake (1999), Distortion of isochronous layers in ice revealed by ground-penetrating radar, *Nature*, (398), 323–326, doi:https://doi.org/10.1038/18653. 1

Waddington, E. D., T. A. Neumann, M. R. Koutnik, H.-P. Marshall, and D. L. Morse (2007), Inference of accumulation-rate patterns from deep layers in glaciers and ice sheets, *Journal of Glaciology*, *53*(183), 694–712, doi:10.3189/002214307784409351. 2, 91

Witt, A., and A. Y. Schumann (2005), Holocene climate variability on millennial scales recorded in greenland ice cores, *Nonlinear Processes in Geophysics*, *12*(3), 345–352, doi:10.5194/npg-12-345-2005. 91

Xingsheng, D., Y. Liangbo, P. Sichun, and D. Meiqing (2015), An iterative algorithm for solving ill-conditioned linear least squares problems, *Geodesy and Geodynamics*, *6*, doi:10.1016/j.geog.2015.06.004. 10

Öztürk, F., and F. Akdeniz (2000), Ill-conditioning and multicollinearity, *Linear Algebra and its Applications*, *321*(1), 295–305, doi:https://doi.org/10.1016/S0024-3795(00)00147-6, eighth Special Issue on Linear Algebra and Statistics. 10

Graphic design: Communication Division, UiB / Print: Skipnes Kommunikasjon AS

uib.no

ISBN: 9788230869062 (print)
9788230855942 (PDF)